Interaction between fine particles and colloidal gas aphrons (CGA)

Inkoo Lee

Department of Mining and Materials Engineering

McGill University

Montreal, Canada

April 2015

A thesis submitted to McGill University

in partial fulfillment of the requirements of the degree of

Master of Science

Abstract

Interactions between fine particles (-10 μm) and colloidal gas aphrons (CGA) were predicted from zeta potential measurements, which were then compared to flotation experiments. CGAs, which are microbubbles coated and stabilized by a surfactant, were used as to selectively recover fine iron oxide or silica particles. Surfactant adsorption was measured by the changes in zeta potential as a function of surfactant addition.

Using synthetic mineral (-10 μm) particles, four sets of recovery experiments were conducted using negatively charged CGA and positively charged CGA (① iron (III) oxide and sodium dodecylsulfate (SDS) CGA, ② silicon dioxide and SDS CGA, ③ iron (III) oxide and hexadecyltrimethylammonium bromide (HTAB) CGA, and ④ silicon dioxide and HTAB CGA). In addition, the recovery of natural fine mineral particles (hematite and quartz) was tested using an identical experiment setups.

Both sets of synthetic particles and natural minerals showed positive correlations between recovery experiments and surfactant adsorption experiments. Therefore, high levels of particle recovery is related to good adsorption of surfactant onto the surface of particles, which is in agreement with electrostatic interactions of particles and CGA. Conversely, low levels of particle recovery is associated with poor

adsorption of surfactant to the surface of particles, which is also explained by their electrostatic properties of similar charge.

After analysis of the experimental data, it is proposed that a particle is attached to a charged microbubble which is generated from an ionic surfactant of opposite charge to the particle. If the particle and CGA have a similar charge, there exists a repulsive electrostatic barrier preventing attachment. A particle's attachment on the charged microbubble showed a strong dependency on the relative electrostatic properties of the particle and charged bubble, with particles able to be selectively attached to charged microbubbles by adjusting both electrostatic properties of particles and bubbles. The current studies of single minerals provided a consistent rationale to explain the results of binary mineral separation experiments by CGA flotation, supporting the dependency on the electrostatic interactions when a bubble and a particle engaged together.

To conclude, a strong dependency on electrostatic properties was found in the behaviors of fine particles to the charged microbubbles, and this phenomena was used for the selective attachment of fine particles to CGAs.

Résumé

Les interactions entre des particules fines (-10μm) et aphrons de gaz colloïdale (AGC) ont été prédits à partir de mesures du potentiel zêta, qui ont comparées à des expériences de flottation. AGC, qui sont des microbulles enrobées et stabilisées par un tensioactif, ont été utilisés pour récupérer sélectivement des particules fines d'oxyde de fer ou de dioxyde de silicium. L'adsorption de tensioactif a été mesurée par les modifications du potentiel zêta en fonction de l'addition de tensioactif.

En utilisant des particules minérale synthétique (-10μm), quatre séries d'expériences de récupération ont été menées en utilisant chargé négativement AGC et chargé positivement AGC (① oxyde de fer (III) et sulfate de dodécyle de sodium (SDS) CGA, ② dioxyde de silicium et SDS CGA, ③ oxyde de fer (III) et le bromure hexadécyle triméthyle ammonium (BHTA) CGA et ④ dioxyde de silicium et BHTA CGA). En outre, la récupération de particules fines minérales naturelles (hématite et de quartz) a été testé en utilisant un configurations expérimentales identiques.

Les deux de particules synthétiques et minéraux naturels ont montré des corrélations positives entre les expériences de la récupération et les expériences de l'adsorption de tensioactif. Donc, des niveaux élevés de récupération des particules sont associés à une bonne adsorption du tensioactif sur la surface des particules, ce

qui est en accord avec des interactions électrostatiques des particules et des AGC . Inversement, de faibles niveaux de récupération des particules sont associés à une mauvaise adsorption du tensioactif à la surface des particules, ce qui se explique aussi par leurs propriétés électrostatiques de charge similaire.

Après analyse des données expérimentales, il est proposé qu'une particule est attachée à un accusé de microbulles qui est généré à partir d'un agent tensioactif ionique de charge opposée à la particule. Si la particule et AGC ont une charge identique, il existe une barrière empêchant l'attachement électrostatique répulsive. L'attachement d'une particule chargée sur le microbulles a montré une forte dépendance sur les propriétés électrostatiques relatives de la particule et la bulle chargée, avec des particules susceptibles d'être montés sélectivement à microbulles chargées en ajustant les deux propriétés électrostatiques des particules et des bulles. Les études actuelles de minéraux simples fourni une justification cohérente pour expliquer les résultats des expériences de séparation de minéraux binaire par la flottation de AGC, en soutenant la dépendance sur les interactions électrostatiques lorsqu'une bulle et une particule engagés ensemble.

Pour conclure, une forte dépendance sur les propriétés électrostatiques a été trouvé dans les comportements des particules fines à microbulles chargées, et ce phénomène a été utilisé pour l’attachement sélective de particules fines aux AGC.

Acknowledgments

I would like to take this opportunity to thank all the people that have aided this project come to life.

Firstly, I would like to acknowledge my supervisor, Professor Kristian E. Waters, for his help and guidance. I would also like to thank Professor James A. Finch for his enthusiasm and kindness, which inspired my work.

I wish to appreciate Mr. Ray Langlois for assistance in developing and setting up the apparatus, and Ms. Monique Riendeau for easy access to the facilities of Materials Engineering Analytical Laboratory and her assistance in the experiments during the study. I would also like to thank Ms. Barbara Hanley for her continuous kindness and administrative support.

I would like to acknowledge other colleagues in the McGill Mineral Processing Group for their constructive suggestions and comments. I appreciate Mr. Zhoutong Deng for translating the abstract of this thesis.

Finally, I would like to thank my family and my wife Jin Seok for support and patience throughout.

Table of Contents

Abstract i

Résumé iii

Acknowledgments v

Table of Contents vi

List of Figures x

List of Tables xiii

1 Introduction 1

1.1 Problem Statement 1

1.2 Objectives 5

1.3 Organization 5

2 Literature Review 6

2.1 Froth Flotation 6

2.1.1 Hydrophobic Forces 8

2.1.2 Effect of Particle Size 11

2.1.3 Flotation Hydrodynamics 13

2.2 Fine Particle Flotation 17

2.2.1 Physical Factors 17

2.2.2 Chemical Factors 18

2.2.3 Slimes Coating 18

2.2.4 Techniques of Fine Particles Flotation 20

2.3 Colloidal Gas Aphrons (CGA) 23

2.3.1 Structure of CGA 24

2.3.2 Characteristics of CGA 25

2.3.3 Generation of CGA 28

2.3.4 Application of CGA 28

2.4 Electrical Double Layer 30

2.4.1 Zeta Potential 31

2.4.2 Oxide Mineral - Water Interfaces 33

2.4.3 Point of Zero Charge and Isoelectric Point 35

2.5 Flotation of Iron Oxide 38

2.5.1 Physical Adsorption on Iron Oxide 39

2.5.2 Chemisorption and Surface Reaction/Precipitation on Oxide Minerals 42

2.5.3 Reagents for Iron Oxide Flotation 42

2.5.4 Direct Flotation of Iron Oxide Ore 44

2.5.5 Reverse Flotation of Iron Oxide Ore 46

3 Experimental Methodology 48

3.1 Materials 48

3.2 Determination of Critical Micelle Concentration 50

3.3 Half Life and Gas Holdup of Microbubbles 51

3.4 Recovery of Fine Particles with CGA Flotation System 53

3.5 Zeta Potential Measurements 56

3.6 Separation of Binary Fine Minerals by CGA Flotation System 60

4 Results and Discussion 62

4.1 Surface Tensions of Surfactant Solutions 62

4.2 Half Life and Gas Holdup of CGA 64

4.3 Synthetic Minerals 67

4.3.1 Zeta Potential of Fe_2O_3 and SiO_2 67

4.3.2 Anionic Surfactant (SDS) System 68

4.3.3 Cationic Surfactant (HTAB) System 74

4.3.4 Separation of Synthetic Binary Fine Minerals 78

4.4 Natural Minerals 85

4.4.1 Zeta potential of Hematite and Quartz 85

4.4.2 Anionic Surfactant (SDS) System 86

4.4.3 Cationic Surfactant (HTAB) System 90

4.4.4 Separation of Natural Binary Fine Minerals 94

5 Conclusions and Recommendations for Future Work 100

5.1 Conclusions 100

5.2 Recommendations for Future Work 102

References 104

Appendix 112

List of Figures

Figure 1. Proposed structure of CGA by Sebba 3

Figure 2. Illustration of flotation principles in a mechanical cell 7

Figure 3. Contact angle between bubble and particle in an aqueous medium 10

Figure 4. Variation of flotation recovery with particle size 12

Figure 5. Stern model of electrical double layer 31

Figure 6. Dependence of goethite flotation on surface charge 40

Figure 7. Illustrative interactions of surface-active organic compounds at the electrical double layer 41

Figure 8. Electrophoretic mobility and flotation results 45

Figure 9. Experimental set up for half life and gas holdup measurement 51

Figure 10. Schematic of the CGA flotation column system 53

Figure 11. Surface tensions of surfactant solutions (SDS and HTAB)..... 62

Figure 12. Half life and gas holdup of SDS CGA 64

Figure 13. Half life and gas holdup of HTAB CGA 65

Figure 14. Zeta potential of Fe_2O_3 and SiO_2 as a function of pH 67

Figure 15. Fe_2O_3 recoveries by SDS CGA flotation as a function of pH, and comparison of Fe_2O_3 zeta potential..... 68

Figure 16. SiO_2 recoveries by SDS CGA flotation as a function of pH, and comparison of SiO_2 zeta potential..... 70

Figure 17. Zeta potential of Fe_2O_3 as a function of pH at different SDS concentrations 71

Figure 18. Zeta potential of SiO_2 as a function of pH at different SDS concentrations 73

Figure 19. Fe_2O_3 recoveries by HTAB CGA flotation as a function of pH, and comparison of Fe_2O_3 zeta potential at different HTAB concentrations..... 75

Figure 20. SiO_2 recoveries by HTAB CGA flotation as a function of pH, and comparison of SiO_2 zeta potential at different HTAB concentrations..... 76

Figure 21. Grade-recovery of Fe_2O_3 by SDS CGA flotation..... 79

Figure 22. Grade-recovery of Fe_2O_3 by HTAB CGA flotation 81

Figure 23. Comparison of cumulative recovery of binary mineral feeds (synthetic) separated by HTAB CGA and the average respective recoveries of Fe_2O_3 and SiO_2 84

Figure 24. Zeta potential of hematite and quartz as a function of pH..... 85

Figure 25. Hematite recoveries by SDS CGA flotation as a function of pH, and comparison of hematite zeta potential at different SDS concentrations 87

Figure 26. Quartz recoveries by SDS CGA flotation as a function of pH, and comparison of quartz zeta potential at different SDS concentrations 88

Figure 27. Hematite recoveries by HTAB CGA flotation as a function of pH, and comparison of hematite zeta potential at different HTAB concentrations..... 90

Figure 28. Quartz recoveries by HTAB CGA flotation as a function of pH, and comparison of quartz zeta potential at different HTAB concentrations 92

Figure 29. Grade-recovery of hematite by SDS CGA flotation..... 94

Figure 30. Comparison of cumulative recovery of binary mineral feeds (natural) separated by SDS CGA and the average of respective recoveries of hematite and quartz..... 98

Figure 31. Grade-recovery of hematite by HTAB CGA flotation 99

List of Tables

Table 1: PZC of some oxides 36

Table 2: PZC, and IEP of the iron oxides 37

Table 3: Characteristics of the particles used in the study 48

Table 4: List of surface tension measurement experiments 50

Table 5: List of half life and gas holdup measurement experiments 52

Table 6: List of recovery experiments with synthetic minerals 55

Table 7: List of recovery experiments with natural minerals 55

Table 8: List of zeta potential measurement experiments with synthetic minerals 57

Table 9: List of zeta potential measurement experiments with natural minerals.. 57

Table 10: List of separation experiments with synthetic minerals..... 60

Table 11: List of separation experiments with natural minerals 60

Table 12: Comparison of synthetic mineral flotation results by HTAB CGA..... 82

Table 13: Comparison of natural mineral flotation results by SDS CGA 96

1 Introduction

1.1 Problem Statement

Developing technologies in mineralogy, grinding and flotation has allowed the exploitation of large amounts of low grade ores. To utilize such types of complex ores, increasing amount of fine particles are generated and processed (Chadwick, 2003). The fines, *i.e.* particles of sizes below 10 μm (Trahar, 1981), are sometimes the required size for adequate liberation in case of low quality ores, but, more often, they are parts of a stream of which the coarser particles are the main focus of a process, and as such are removed in a desliming process, which leads to the loss of some value material. There are many examples of the processing systems that require a deslimed feed for operations (Somasundaran, 1986), therefore the studies of separating fine particles are beneficial for utilizing finely grained ores as well as recovering value from slime.

Fines have characteristics distinct from coarser particles, notably in hydrodynamics. This is one of the reasons that the 0 - 10 μm fraction has a lower recovery than for the intermediate fraction (Johnson, 2006; Trahar and Warren, 1976). In flotation, mineral particles must collide to, adhere to, and not detach air bubbles in order to be floated successfully. The decreasing particle-size makes the collision less likely, therefore, fine particles generally show low recovery due to a low probability of collision with bubbles (Yoon, 2000).

The probability of attachment determines selectivity of flotation, which is largely governed by surface forces, such as electrostatic and hydrophobic ones. When particles and bubbles are oppositely charged, the electrostatic attraction forces help to form bubble-particle aggregates. The role of hydrophobic forces is to make stable attachment of a particle to a bubble with rupturing of the air-water interface around bubbles. The probability of detachment in fine particle flotation is negligible because of the fines' low inertia (Yoon, 2000).

Many studies have focused on using small bubbles in order to achieve enhanced separation of fines by increasing the probability of bubble-particle collision. Dissolved air flotation (Yalcin and Byers, 2006), picobubble flotation (Tao *et al.*, 2006), and colloidal gas aphrons (CGA) flotation (Waters *et al.*, 2008) have reported improved separation of fines. Among the improved flotation techniques suggested, CGA flotation is unique in utilizing the surface charge of fine bubbles, which introduces the potential of selective adherence of particle to bubbles based upon electrostatics.

Colloidal gas aphrons are microbubbles (10 ~ 100 μm) encapsulated by a soapy film. It is believed to consist of multi-layers of surfactant molecules with a gas core at the center, and the postulated structure of CGA is presented in Figure 1. CGA dispersions can be generated by intensive stirring of surfactant solutions with a disc impeller in a baffled container (Sebba, 1987).

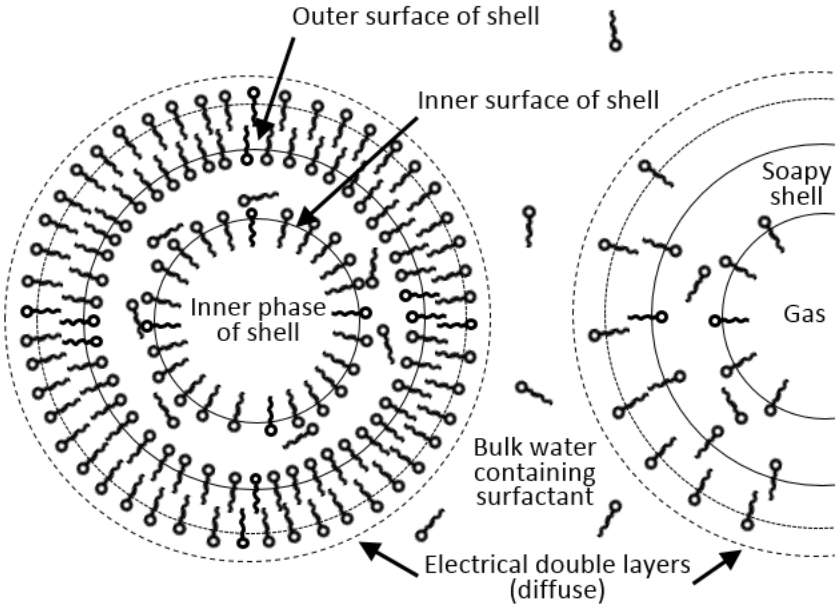

Figure 1. Proposed structure of CGA by Sebba (reproduced from Sebba, 1987)

CGA have some attractive characteristics for flotation, such as: 1) large interfacial areas; 2) high stability; 3) controllable surface charge (Fuda and Jauregi, 2006). CGA's small size makes the large interfacial area, which lead to higher probability of bubble-particle collision. The CGA foam generated, termed the dispersion, is relatively stable due to the multi-layer structure of the individual CGA, so it can be pumped like a liquid. This enables the separation of the CGA generator from a flotation column, so modification of the CGA characteristics is not restricted by the environment of flotation column. In addition, the surface charge of CGA can be modified depending on the types of surfactants used for its generation. For example, sodium dodecylsulfate (SDS), an anionic surfactant, forms negatively charged CGA, and hexadecyltrimethylammonium bromide (HTAB), which is a cationic

surfactant, generates positively charged CGA. The use of a non-ionic surfactant, such as Polysorbate 80, results in an uncharged CGA. Accordingly, the probability of adherence in CGA flotation is not limited by hydrophobic forces, but the electrostatic forces between particle and bubble.

CGA flotation has been proposed for a number of applications including: protein separation and recovery (Fuda and Jauregi, 2006; Noble *et al.*, 1998); separation of organic dyes from waste water (Roy *et al.*, 1992); removal of heavy metal ions from water (Ciriello *et al.*, 1982); and fine mineral separation (Waters *et al.*, 2008). The study by Waters *et al.* (2008) included a comparison between CGA flotation and conventional flotation with feeds of a mixture of copper (II) oxide and silicon dioxide, and zeta potential analysis of the two mineral particles. They used anionic SDS CGA and reported superior separation results of CGA flotation to those by a Denver cell, and the study of zeta potential suggested that electrostatic interactions are as a main driver of the attraction/repulsion between SDS CGA and fine mineral particles. Further, they concluded that the exploitation of electrostatic interactions has potential for the selective separation of fine mineral feedstock. Johnson *et al.* (2009) then used atomic force microscopy (AFM) and measured the forces between silica probe and microbubbles generated by anionic SDS and cationic DTAB (dodecyl trimethylammonium bromide). They found that repulsive long-range interactions were responsible for the selective attachment of silica particles to microbubbles in a charge-dependent manner.

1.2 Objectives

The purpose of this study was to understand nature of interactions between fine mineral particles and CGA at the CGA flotation system, and apply it to the selective separation of fine particles by CGA flotation system. The study of particle-CGA interaction was conducted by correlating the results from particle recovery by CGA flotation system and surfactant adsorption measured by zeta potential analysis. Finally the separation of bi-mineral feeds was conducted by CGA flotation system, and the results were interpreted based on the study of particle-CGA interaction.

1.3 Organization

This thesis is organized into 5 Chapters. Chapter 1 gives an introduction to the thesis itself. Chapter 2 reviews prior research relating to the studies of this thesis, followed by Experimental Methodology in Chapter 3. The final section of the thesis includes Results and Discussion in Chapter 4 and ends with Conclusions and Recommendations for Future Work in Chapter 5.

2 Literature Review

2.1 Froth Flotation

Flotation was initially developed over 100 years ago to separate valuable sulphides from unwanted gangue minerals in deposits of increasing complexity, which rendered previous techniques impractical due to more complex types of ores. Currently a wide variety of ores are processed using flotation, including oxides, oxidised minerals, and non-metallic ores (Wills, 2006). Flotation of iron-oxide is discussed in more detail in Section 2.5.

In a flotation system, valuable minerals report to the concentrate by either true flotation or entrainment. True flotation is the most important mechanism, which represents a mineral's selective attachment to air bubbles. Entrainment is non-selective process, therefore both valuable minerals and gangue report to the concentrate by entrainment. Although the main process is true flotation, entrainment increases the recovery of valuable minerals whilst lowering the grade (Wills, 2006). In industrial flotation practice, the effect of entrainment is controlled by adopting several stages of flotation (Cooper *et al.*, 2004; Hadler and Cilliers, 2009).

The key driver for true flotation is the difference in surface properties of mineral particles. To reach the required degree of difference in physico-chemical surface properties, the flotation pulp is conditioned with reagents, such as collector and

depressant. The details about electrical property of particle surface are discussed in Section 2.4, and the interaction mechanism of reagents and the types of reagents for iron oxide flotation are discussed in Section 2.5.

When a particle can attach itself to an air bubble, it is lifted to the water surface by the bubbles. The principles of flotation in a mechanical cell is illustrated in Figure 2. The agitation promote collision of particles and bubbles by creating turbulence in the pulp phase. Valuable particles are attached to bubbles, and the bubbles transport them into the concentrate. The hydrodynamics of flotation is discussed in Section 2.1.3.

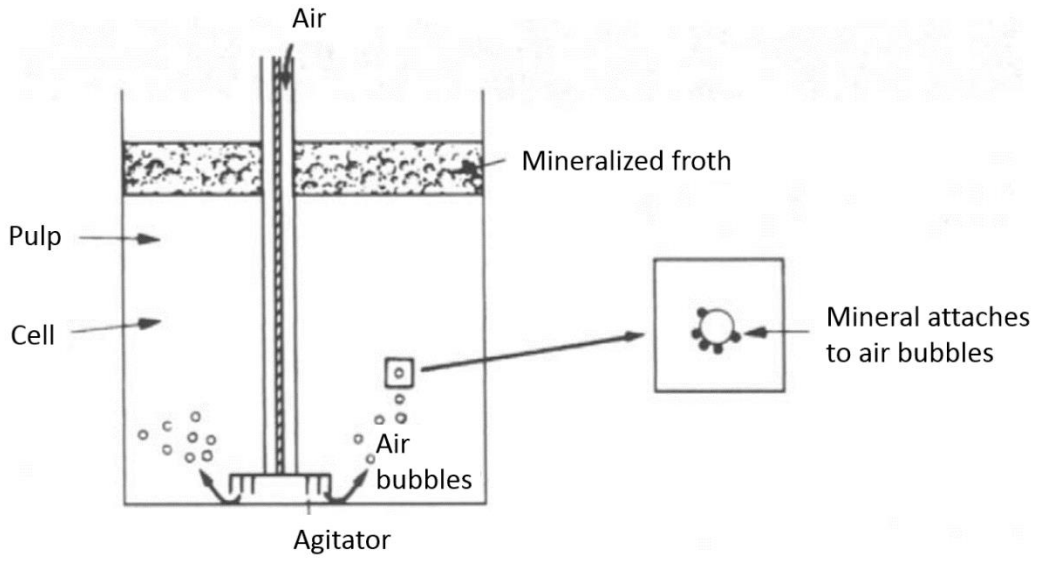

Figure 2. Illustration of flotation principles in a mechanical cell (Wills, 2006)

There is an optimum range of particle sizes in which the flotation process can be applied effectively. In case of large particles, the particle weight may overcome the adhesive force between the bubble and the particle, therefore the particle will become detached from the bubble.

The flotation process can be categorized to direct flotation or reverse flotation depending on the particles transferred to the froth. In direct flotation, valuable minerals are loaded on the surface of bubbles and carried to the float fraction, leaving the unwanted gangue in tailing. In reverse flotation, the gangue is preferentially floated, which is the opposite of direct flotation.

2.1.1 Hydrophobic Forces

Hydrophobic mineral surfaces, and stability of the bubbles are important factors for the successful separation by flotation. The desired particles can only be attached to and carried by the air bubbles when they are hydrophobic, or water-repelling. The bubbles should form a stable froth and support the particles until arriving at the surface and overflowing. To control these conditions, the numerous flotation reagents are used.

Laskowski and Kitchener (1969) first recognised the role of hydrophobic forces on particle-bubble interaction. They employed both negatively charged bubbles and silica plates, which were hydrophobized by trimethylchlorosilane (TMCS). Although the van der Waals forces in the wetting zone were found to be repulsive,

they observed those bubbles immediately attached to the hydrophobic silica plate, and a large contact angle was observed (70 - 80°). After the electrostatic and van der Waals dispersion force, they suspected the presence of a third force which causes adhesive interaction between bubbles and particles.

As hydrophobic forces are very strong, it was once believed that there existed a 'hydrophobic bond' accounting for it (Kauzmann, 1959); however it is now acknowledged that as two hydrophobic species approaching it is associated with configurational rearrangement of water molecules, therefore the hydrophobic forces has the longer ranges than a typical covalent bond (Ben-Naim *et al.*, 1973; Dashevsky and Sarkisov, 1974). Later, Israelachvili and Pashley (1982) directly measured the distance dependence and effective range of hydrophobic forces. They found that hydrophobic interaction has the same range as the van der Waals force, but with a stronger magnitude, and that hydrophobic interaction decays exponentially in 0 - 10 nm range with a decay length of ~ 1 nm.

The forces acting on the surface of mineral and bubble are responsible for the interaction between mineral and bubble. Schematics of the forces at the surface of a particle and a bubble are represented in Figure 3, and this three phase contact is defined with thermodynamic conditions by Young's Equation. An angle between the surface of mineral and bubble is generated by tensile forces.

$$\gamma_{s/a} = \gamma_{s/w} + \gamma_{w/a} \cos\theta \tag{2.1}$$

Where $\gamma_{s/a}$, $\gamma_{s/w}$, and $\gamma_{w/a}$ are the tensions of the solid and air, solid and water, and water and air, respectively, and θ is the contact angle. The contact angle is the angle between the water-air and the solid-water interfaces, measured through the water.

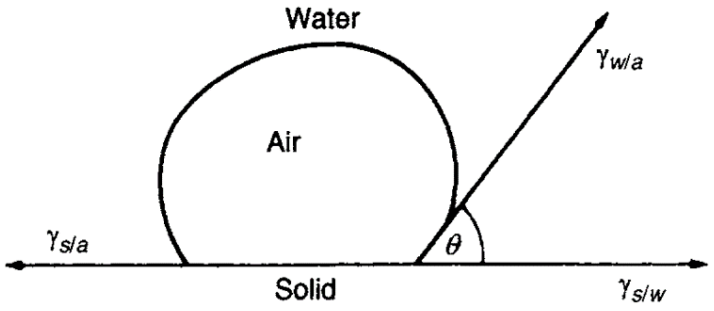

Figure 3. Contact angle between bubble and particle in an aqueous medium (Wills, 2006)

The work of adhesion is the force required to break solid-air interface. This requires the replacement of a unit area of solid-air interface by solid-water and water-air interfaces, and the work of adhesion is given by Dupre's Equation:

$$W_{s/a} = \gamma_{s/w} + \gamma_{w/a} - \gamma_{s/a} \tag{2.2}$$

Combining Young's Equation with Dupre's Equation gives the following expression for the work of adhesion:

$$W_{s/a} = \gamma_{w/a}\,(1 - \cos\theta) \tag{2.3}$$

With large contact angles, the work of adhesion is increased. Therefore the three phase contact system becomes more resilient to disruptive forces, and a mineral is deemed more hydrophobic with larger contact angles.

There are limitations to the theories, with Dupre's Equation not considering the geometry of the system (Fuerstenau and Raghavan, 2007; Johnson, 1959), and Young's Equation only working in an ideal situation such that there is no gravitational effects within the system at equilibrium (Fuerstenau and Raghavan, 2007; Johnson, 1959). Hysteresis in measurements of contact angle shows that the system is not in equilibrium, and the typical causes of the hysteresis is known to be surface contamination, roughness, nonequilibrium adsorption, to name but a few (Adamson and Gast, 1967; Wakamatsu and Fuerstenau, 1973).

2.1.2 Effect of Particle Size

Gaudin *et al.* (1931) first made detailed studies on particle size as a factor of the flotation performance. After studying the flotation process of a number of sulphide concentrators, they concluded that particles with diameters between 10 and 50 μm are optimal for the recoveries of lead, zinc, and copper sulphides. They sized the product by elutriation, and the sizes are the equivalent of quartz spheres. Figure 4 summarizes their work, and shows asymmetric shape of the recovery-size curves. The results from other mills and laboratory batch test were also investigated, and

similar behaviour has been found. The conclusion is reached that an intermediately sized particles show the best recovery (Trahar and Warren, 1976).

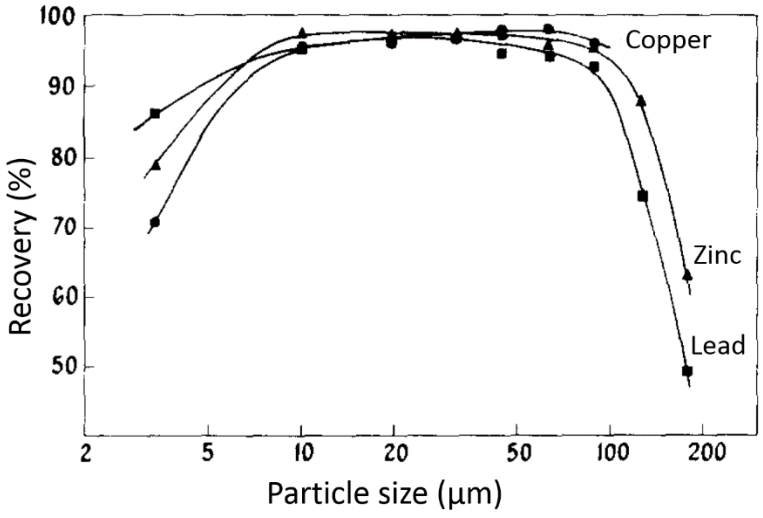

Figure 4. Variation of flotation recovery with particle size (from Trahar and Warren (1976), and data originally from Gaudin *et al.* (1931))

Different minerals show a variation of optimal size range for maximum recovery. Trahar studied the size-by-size floatability of minerals and founded the optimum particle sizes for the maximum recovery; for example, galena (6-70 µm), sphalerite (8-90 µm), pyrrhotite (9-40 µm), chalcopyrite (15-60 µm), arsenopyrite (15-120 µm) and pyrite (20-150 µm). By comparing laboratory batch flotation with full scale continuous flotation, he concluded that the relative behaviour of the different sizes of particle showed good agreement for both recovery results from laboratory and industrial mill (Trahar and Warren, 1976).

As found from the asymmetric shape of the recovery-size curve, the rationales behind these observations are attributed to different mechanism. The low likelihood of bubble-particle collision is the main cause of low recovery of fine particles, whereas significant detachment is responsible for the low performance of coarse particles (Trahar and Warren, 1976).

2.1.3 Flotation Hydrodynamics

Collision, attachment, and detachment are the important interactions between particles and bubbles in a flotation cell, and successful flotation results only if a proper combination of these activities are achieved. The collision of the particles with air bubbles does not necessarily result in successful flotation, but hydrophobicity of particles is required for attachment and selective flotation to occur. Therefore, the probability of attachment is a determinant of the selective flotation process, whereas the probability of collision performs a critical role on recovery. Further, particles are sometimes disassociated from the air bubbles due to the inertia force of particles and turbulence in the flotation cell. In a flotation cell, the surface chemistry of the bubbles and particles largely determines the processes of the attachment and detachment. However, the surface chemistry parameters, such as zeta potential, contact angle, Hamaker constant, etc. are not enough to predict these activities, therefore detailed studies of flotation hydrodynamics should be considered (Yoon, 2000).

Denoting the probability of flotation as P_f, it can be combined with the probability of bubble particle collision (P_c), the probability of attachment (P_a), and the probability of detachment (P_d), and given by:

$$P_f = P_c \ P_a \ (1 - P_d) \tag{2.4}$$

P_d can be neglected in case of fine particle flotation because of fine's low inertia. In this case, Equation 2.4 becomes:

$$P_f = P_c \ P_a \tag{2.5}$$

The major determinants of P_c are bubble size, particle size, and the turbulence at the flotation cell whereas P_a is largely associated with surface chemistry as well as hydrodynamics (Dobby and Finch, 1987).

2.1.3.1 Probability of collision

The probability of collision performs an important role on recovery, and is determined by the hydrodynamics in a flotation cell. Sutherland (1948) studied the relationship between the diameter of the particle (D_p) and the diameter of the bubble (D_b) for the P_c and expressed it as

$$P_c = 3 \ D_p \ / \ D_b \tag{2.6}$$

Because Equation 2.6 assumes potential flow in the system, it is only reasonable when D_b is much bigger than what is observed in the flotation cell.

Assuming Stokes flow condition, a relationship for P_c was derived by Reay and Ratcliff (1973);

$$P_c \propto \left(D_p \,/\, D_b\right)^2 \tag{2.7}$$

After being applied experimentally, Equation 2.7 has been verified for the fine particle flotation (Yoon, 2000). As seen in Equation 2.7, the probability of collision increases with particle diameter and with decreasing bubble diameter.

2.1.3.2 Probability of attachment

Bubble-particle attachment is assumed to occur when the intervening liquid film thins and ruptures by the particle which has collided and is sliding over the rising bubble. The induction time (t_i) is defined as the time required for the disjoining film to rupture. Therefore, particles with greater sliding time than induction time are assumed to have attached (Dobby and Finch, 1987).

Based on this assumption, Yoon and Luttrell (1989) derived an equation for P_a,

$$P_a = \sin^2\left[2\tan^{-1}\exp\left\{\frac{-\left(45+8Re^{0.72}u_b t_i\right)}{15D_b\left(D_b \,/\, D_p\ +1\right)}\right\}\right] \tag{2.8}$$

Where t_i is the induction time and u_b is the rise velocity of the bubble (Yoon, 2000). The induction time is largely affected by various reagent conditions, therefore a function of particle hydrophobicity. Equation 2.8 implies the effect of bubble size and particle size on the probability of attachment. When particle size decreases, the

particle and air bubble are more likely to be attached. If bubble size decreases to a certain level, P_a increases due to reduced rise velocity (U_b) of the bubble. If the size of bubble further decreases and gets too small, P_a starts to decrease due to decreased sliding distance along the surface of the bubble (Yoon and Luttrell, 1989).

2.2 Fine Particle Flotation

As particle size decrease significantly, the chemical and physical parameters in the flotation cell are altered. Consequently, recovery drops in the conventional conditions of flotation, which focuses on the maximum recovery of intermediately sized particles (Trahar and Warren, 1976).

2.2.1 Physical Factors

The main principal factor to consider in fine particle flotation is the low probability of collision between a particle and bubble. As discussed in Section 2.1.3.1, it is necessary for a particle to collide with a bubble for successful flotation. If the momentum of the solid particles is too low, it is likely to follow the water streamline around a bubble and fail to make direct contact with a bubble. Hence the momentum of a fine particle should be sufficient to overcome the water flow around the bubble.

The attachment of a particle to a bubble is affected by the particle size. As discussed in Section 2.1.3.2, induction time should be shorter than the time taken for the particle to slide over the surface of a bubble. Otherwise, the successful attachment might not occur. When particle size decreases, the particle and air bubble are more likely to be attached each other. If the bubble size decreases while maintaining enough sliding surface for a particle, the probability of attachment increases as a result of reduced rise velocity of the bubble (Rao, 2004).

2.2.2 Chemical Factors

Fine particle flotation is influenced by several chemical factors, originating from interfacial phenomena, as well as the bulk and solution chemistry. The main factors to be considered are high specific surface area, collector concentration, solubility effect, and surface charge effects. High specific surface area leads to high adsorption capacity, and large amounts of reagent are consumed by fine particles. High adsorption capacity results in low recovery due to consumption of collectors, and large surface energy leads to lower grade due to nonselective adsorption (Rao, 2004).

2.2.3 Slimes Coating

Slimes coating is when fine particles coat a large ore, giving a “pseudo-surface”. In flotation of a mineral with negative surface charge, for example, if there are slimes with positive surface charge, valuable mineral surfaces must be coated with slimes due to electrostatic attraction. Slimes coating retards collector adsorption, and flotation is inhibited. An example is the case of quartz flotation by dodecyl ammonium acetate by Fuerstenau and coworkers (1958). They initially had higher recovery of quartz in the absence of slimes, but found that the flotation was discouraged with in addition of iron oxide slime at pH lower than 9.5. Slimes coating was only observed at pH 9.5 or lower. For desliming, the pulp was conditioned at higher pH which leads to a negative surface charge of iron oxide

slime, and the flotation was improved. In addition, the use of dispersing agents increased flotation performance; for instance, addition of sodium hexametaphosphate increases the double-layer charge and counter ion association, therefore achieving electrostatic stabilization. In some instances, ultrasonic treatment is adopted for dispersing slime layers above pH 9.5 where the surface charge of slimes becomes negative (Rao, 2004).

Fuerstenau (1980) compared the flotation results of a number of minerals, and found that slimes coating is not likely to affect significantly when chemisorbing collectors are in use, but prevents flotation at the use of physically adsorbing collectors. It is difficult to generalize, but some cases were reported that adaptation of chemisorbing collectors offset adverse effects of slimes coating which was prevailing at the mechanism of physically adsorbing collectors. In hematite flotation, for instance, the conventional process is to float hematite using sulfonate anionic collector which adsorbs electrostatically. To obtain good selectivity, a desliming process is required, and significant loss of hematite occurs. Fuerstenau *et al.* (1970) used a chemisorbing chelating agent, octyl hydroxamate, and achieved 86% recovery and a concentrate grade of 64% Fe. The specific chemical interaction between hematite and hydroxamate seems to form a strong chemisorption bond, and the hematite becomes strongly hydrophobized, which has overcame the electrical attraction between hematite and quartz.

2.2.4 Techniques of Fine Particles Flotation

Conventional flotation systems sometimes do not work efficiently with fine particles, hence many types of modification have been introduced to flotation process. Carrier flotation was first developed for the removal of colloidal impurities from wastewaters, and adopted to mineral processing. Its name "carrier" comes from the mechanism that the added mineral carries fine minerals for separation. The types of carrier material can be coarser particles, either of the same mineral or another compound, but the carrier material should physically attract the fines by electrostatic or van der Waals interaction similar to slimes coating (Rao, 2004; Wang and Somasundaran, 1980).

Oil assisted flotation is based on the principle of wettability using bulk oil. Earlier flotation practice was conducted with oil until soluble collectors were introduced to the mineral flotation process. In the three phase system of water, oil and solid, the solid will be attached at the oil-water interface in either cases that interfacial tension of oil-water interface is greater than the sum of surface tensions between solid-oil and solid-water phase, or that there are not any respective interfacial tensions which is greater than the sum of the rest two (Greene and Duke, 1962; Rao, 2004). Shergold and Mellgren (1969) utilized this technique for processing fine mixtures of hematite and quartz. They prepared a pulp by dispersing fine particles in water and injected fine droplets of iso-octane oil into the pulp. The oil droplets loaded with fine mineral particles were recovered with the aid of air bubbles.

Because the interactions between oil and solids are associated with long range intermolecular force, collection of fine particles by oil-water interface is likely to be easier than by air-water interface (Rao, 2004).

The previous section about hydrodynamics (2.1.3), noted that decreasing bubble size generally increase flotation efficiency for the fine particle separation in terms of recovery and grade. Therefore, generating small bubbles has been the focus of many studies. Electroflotation is a good example of fine bubble flotation which makes use of electrolysis. Ketkar *et al.* (1991) used hydrogen gas bubbles generated from electrolysis and applied them for the electroflotation of fine quartz.

Dissolved air flotation uses the small bubbles generated by pressure release. If pressure is released over a super-saturated solution of air in water, small bubbles are produced due to decreased solubility of air in water, which is in accordance with Henry's Law. Bubbles of 30-100 μm are generated, and very fine bubbles on a particle surface increase the probability of their attachment to larger bubbles. One of the explanations for the high attachment rate is that a small bubble acts as a spearhead on the surface of particle, so the spearhead aids penetration of the hydrated layers around a large bubble (Matis and Gallios, 1986). Yalcin and Byers (2006) used argon gas for dissolved air flotation of copper-nickel ore, and found significantly higher grades and recoveries.

Flotation column was developed in 1980s and became an important technique for fine particle flotation through several modifications. It uses spargers to generate fine bubbles and maintains quiescent conditions in the vessel. Close contact between bubbles and particles are promoted, and wash water rejects hydrophilic gangue particles. In tests, high separation performance is achieved (Dobby and Finch, 1991; Finch and Dobby, 1991). Reportedly, single-stage column cell achieves upgrading which is comparable to what multiple-stage mechanical cells produce (Egan *et al.*, 1988). After adopting modified spargers which generate smaller bubbles, the application of a flotation column can be extended to fine particle flotation. Yoon (1993) made used of an external centrifugal pump and could provide microbubbles into flotation column. It was developed to a Microcel column system and widely used in the industrial practice of fine particle flotation.

Waters *et al.* (2008) adapted colloidal gas aphrons (CGA) for the separations of mineral particles and reported improved separation results compared to conventional flotation results. Colloidal gas aphrons are microbubbles stabilized by surfactants (Sebba, 1987). Due to small size of CGA, the large interfacial area is generated, and bubble particle collision is encouraged. In addition, surface charge of CGA can be utilized for reinforcing selective attachments of particles to CGA.

2.3 Colloidal Gas Aphrons (CGA)

Colloidal gas aphrons are microbubbles (10-100 μm) encapsulated by a soapy film. It is believed to consist of multi-layers of surfactant molecules with a gas core at the center (Sebba, 1987). Conclusive evidence on the structure has not been provided, but there is evidence supporting the CGA's lamellar structures (Jauregi *et al.*, 2000) and structural differences from conventional foams (Feng *et al.*, 2009; Yan *et al.*, 2005). CGA dispersions can be generated by intensive stirring of surfactant solutions with a disc impeller in a baffled container. When a disc impeller rotates at high speed (> 7,000 rpm) the resulting shear forces produce these small bubbles.

The use of CGA for flotation has been proposed for a number of applications including: protein separation and recovery (Fuda and Jauregi, 2006; Noble *et al.*, 1998); separation of organic dyes from waste water (Roy *et al.*, 1992); removal of heavy metal ions from water (Ciriello *et al.*, 1982); and fine mineral separation (Waters *et al.*, 2008). The study by Waters *et al.* (2008) suggested that the attraction and repulsion between CGA and fine mineral particles is initially driven by electrostatic interactions, and the exploitation of electrostatic interactions has potential for the selective separation of fine mineral feedstock.

2.3.1 Structure of CGA

The proposed structure of CGA is presented in Figure 1 (Section 1.1). In the process of their generation, molecules of surfactant adsorb at the interface making their hydrophilic heads towards water phase and leaving tails into the gas phase. Sebba (1987) observed delayed coalescence and, resultantly, extensive stability of CGA in comparison of conventional bubbles as well as other distinct behaviors of CGA. Based on his observations, it was hypothesized that it has different structures from conventional forms, which consists of multi-layers of surfactant molecules with a gas core at the center as described in Figure 1. Still, conclusive evidence has not been provided, but a significant amount of research have been published on the structure of CGA.

Jauregi *et al.* (2000) predicted drainage kinetics of foams with and without modifying structures, and compared them to the observed drainage kinetics of CGA. The best prediction was given by the foams with structural modification, hence supporting Sebba's theory. In addition, Jauregi and coworkers adopted small angle x-ray diffraction, and confirmed the hypothesis that CGA has lamellar structures (Jauregi *et al.*, 2000).

A number of research studied drainage kinetics and highlighted the difference of CGA from conventional forms (Bhatia *et al.*, 2005; Feng *et al.*, 2009; Moshkelani and Amiri, 2008; Save and Pangarkar, 1994; Yan *et al.*, 2005). Among them,

Moshkelani and Amiri (2008) used electrical conductivity measurements and found that CGA drainage occurs in three stages. Previously, CGA was understood to have two stages in their drainage (Save and Pangarkar, 1994; Yan *et al.*, 2005), which is similar to the two-stage drainage of conventional wet forms (Koehler *et al.*, 2000). The study of Feng *et al.* (2009) made use of photomicrographs of CGA and volumes of drained liquid, and three-stage drainage of CGA was further supported. All in all, these research provide evidences that the structure of CGA is different from conventional forms (Jauregi and Dermiki, 2010).

2.3.2 Characteristics of CGA

CGAs have a structure distinct from conventional forms, and show unique properties, such as high stability, adjustable surface charge, and small size.

2.3.2.1 Stability

Due to multilayer structure, a CGA dispersion is very stable. When two conventional bubbles collide, the two surfactant interfaces from each bubble meet and easily break. On the other hands, as observed from Figure 1 (Section 1.1), multiple interfaces are forced to crash in case of CGA collision, each of which is stabilized by surfactant. This multilayer structure supports stability of CGA (Sebba, 1987). A good indicator for stability is measuring drainage rate of the liquid. Half-life (τ) is defined as the time determined to collect half of the volume of surfactant

solution used for generating CGA (Bikerman, 1953). In addition, gas hold-up is used to measure the gas content of CGA. Gas holdup (ε) is defined as the volumetric ratio of gas contents to CGA dispersion, and is calculated from Equation 2.9.

$$\varepsilon = \frac{V_{gas}}{V_{CGA}} \tag{2.9}$$

Equation 2.10 denotes the volume of gas contents from Equation 2.9 where V_{CGA} and $V_{initial\ liquid}$ represent the final volume of CGA and the volume of solution used for generating CGA, respectively.

$$V_{gas} = V_{CGA} - V_{initial\ liquid} \tag{2.10}$$

The stable nature of CGA enables transportation of CGA by pumping. Although conventional foams usually lose their initial characteristics while pumping, CGA maintains its properties against pumping process. This enables the separation of the CGA generator from a flotation column, so the modification of CGA characteristics is not restricted by the environment of flotation column.

2.3.2.2 Surface charge

Depending on the types of surfactants, the surface charge of CGA can be modified. For instance, negatively charged CGAs are generated when an anionic surfactant, such as sodium dodecylsulfate (SDS), is used. When cationic hexadecyltrimethylammonium bromide (HTAB) is used, positively charged CGAs are produced. Also, the use of non-ionic surfactant, for example Polysorbate 80,

results in un-charged CGA. Accordingly, the probability of attachment is not limited by hydrophobic forces, but the electrostatic forces also can affect selective attachment (Jauregi and Dermiki, 2010).

The experiments by Waters *et al.* (2008) and Johnson *et al.* (2009) support the discriminative nature of electrostatic forces depending on the surface charges of particles and CGA. In the works of Waters *et al.* (2008), copper (II) oxide and silica were separated by negatively charged SDS CGA. They suggested that the attraction between CGA and fine mineral particles is initially driven by electrostatic interactions. Johnson *et al.* (2009) reported that repulsive long-range interactions cause silica particles to be attached on the surface of charged microbubble in a charge-dependent manner. They generated CGA with anionic SDS and cationic DTAB (dodecyl trimethylammonium bromide), respectively, and measured the forces between silica probe and the CGA by use of atomic force microscopy (AFM). From their experiments, they found that there exists barriers introduced by unfavorable electrostatic interactions between negatively charged silica and the anionic CGA, which was not observed when the cationic CGA was used. Therefore the adverse effect of the same charge imposes resistance when a particle of negative surface charge is approaching to the anionic CGA, and prevents the particle from being attached to the CGA.

2.3.2.3 Small size

CGAs have a large interfacial area per unit volume due to the small bubble size, and this leads to more capacity for attaching and carrying fine particles. In addition, the small bubble size suggests improvements in hydrodynamics, promoting bubble-particle collision as detailed in Section 2.1.3. Factors known to affect the size of bubble include surfactant concentration, ionic strength, the power inputs for CGA generation and the presence of impurities (Torrecilla, 1997).

2.3.3 Generation of CGA

Sebba (1987) recommended that the generation of CGA requires a horizontal disc which rotates rapidly (> 7,000 rpm) between baffles. The disc impellor generates waves beating surfactant solution against baffles, and produce micro foams. Xu *et al.* (2008) compared two methods of CGA generation; one by mechanical agitation and another by sonication. The experiments by both methods lead to the conclusion that sonication method is more efficient with more gas hold-up, finer bubble size, and larger interfacial area. On the other hand, Jauregi and Dermiki (2010) determined that using sonication is expensive and hard to scale up.

2.3.4 Application of CGA

As the properties of CGAs show potential to improve attachment and carrying capacity of materials, researchers have conducted various experiments on

applications of CGAs. For example, CGAs have been applied for biological product process, and it was used for separating proteins (Fuda and Jauregi, 2006; Noble *et al.*, 1998). Other interesting application of CGA is in environmental applications such as soil remediation (Boonamnuayvitaya *et al.*, 2009; Choi *et al.*, 2009; Couto *et al.*, 2009; Park *et al.*, 2009) and water treatment (Ciriello *et al.*, 1982; Roy *et al.*, 1992). Choi *et al.* (2009), and Park *et al.* (2009) showed enhanced results of biodegradation of organic contaminants by making CGA to deliver oxygen and inorganic nutrients to the subsurface area. Roy *et al.* (1992) used CGAs to separate organic dyes from waste water, and Ciriello *et al.* (1982) removed heavy metal ions from industrial effluent.

Extraction of valuable minerals from ores is another industrial aplication that CGA has potential to improve the process. Waters *et al.* (2008) demonstrated the separation of copper (II) oxide (d_{50} = 30 μm) from the mixture with silica (d_{50} = 1.2μm) by CGA flotation using anionic surfactant SDS. They showed improved results compared to those by conventional flotation, and found that the attractive interaction between the anionic CGA and cooper (II) oxide particles is firstly driven by electrostatic interactions. Later, Johnson *et al.* (2009) observed unfavorable electrostatic barriers between a negatively charged particle and anionic CGA, which was not found between the identical particle and cationic CGA. Their studies further supports that electrostatic interactions have potential for the selective separation of valuable minerals from the gangue.

2.4 Electrical Double Layer

The process of finding electroneutrality starts at the moment when minerals are suspended in water. When minerals are immersed in water, a solid-water interface is created, and the surface of solid is saturated by water. As ions derived from the solid, charged species in the suspension are transferred across solid-water interface, and equilibrium is reached. Electrical double layers govern adsorption phenomena at mineral-water interfaces in most of nonsulfide minerals. Hence, interaction between collector and the surface of mineral is largely affected by the chemistry in the water and ion adsorption (Rao, 2004).

Figure 5 shows an illustration of the Stern model of electrical double layer at a solid-water interface, with the left showing extending counterions into liquid phase, and the right presenting dropping potential along the distance from the surface of solid. The closest distance possible (δ) for counterions to approach to the surface is termed the Stern plane. While counterions become hydrated or dehydrated upon adsorption, further subcategorization into inner and outer Stern planes could be defined (Grahame, 1947), but such a distinction is not normally required in studies of flotation chemistry with mineral-water interfaces (Fuerstenau and Raghavan, 2007). The symbols ψ_o and ψ_δ represent the potentials at the surface and at the Stern plane, respectively, and the potential decrease to zero in the bulk of solution.

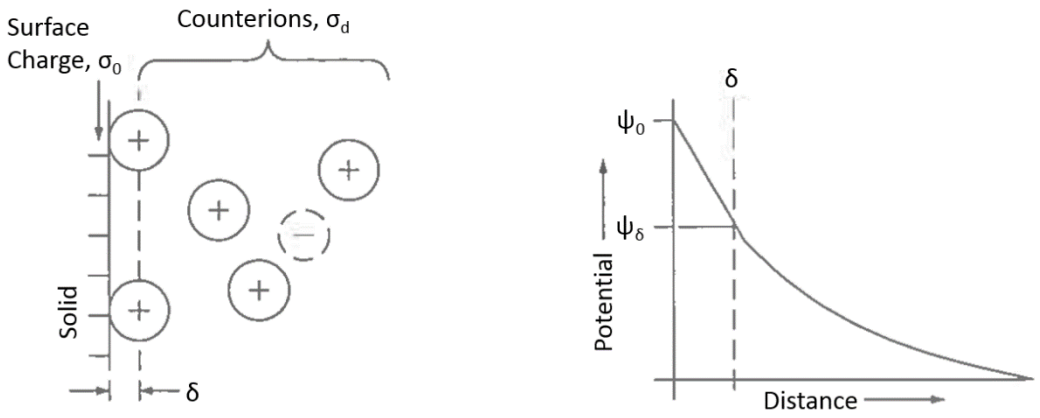

Figure 5. Stern model of electrical double layer (Fuerstenau and Raghavan, 2007)

2.4.1 Zeta Potential

In this chapter of literature review, the term 'zeta potential, ζ (mV)' is used as an approximation of the Stern potential (ψ_δ), and both are applied interchangeably. The concept of zeta potential came after consideration of electrokinetic phenomena in the system of flowing or agitated suspension, which is major area of interest from the colloid science and surface chemistry. The electrokinetic phenomena is defined as the combined effects of mechanical movement of suspension and electrical effect around the particles. As the definition of electrokinetic implies, the movement of particle is accompanied by same movement of thin layer of surrounding liquid due to hydrodynamic shear. The distance from the surface of solid to the end of the stationary liquid layers around particle is called the plane of shear, otherwise, the

surface of shear or slipping plane. Zeta potential is the potential at the surface of shear, and the magnitude of the zeta potential is considered to be close to the Stern potential (ψ_δ). Similarly, the location of the plane of shear is usually considered as equivalent to the Stern layer. These approximations are assumed to be reasonable because the difference of potentials at the surface of shear and at the Stern layer is small when it is compared with the potential difference across the double layer (Rao, 2004).

When the electrochemical potential of these ionic species stays constant throughout the system, equilibrium is attained. Electrochemical potential is written as:

$$\bar{\mu} = \mu + vF\varphi \tag{2.11}$$

where μ is the chemical potential of the species, v is the valency (charge) of the ion, F is the Faraday constant, and ϕ is the Galvani potential in the phase. The ions which pass between the two phases and establish the electrical double layer are called as potential determining ions. The potential determining ions in case of oxide minerals are H^+ and OH^- ions, and the magnitude and sign of the zeta potential are determined by the concentrations of potential determining ions.

2.4.2 Oxide Mineral - Water Interfaces

Electrical double layer is controlled by ions, which freely pass through interface of solid and liquid. Generally, the development of charge at the surface of oxide minerals is expressed as Equations 2.12 and 2.13.

$$MOH_{(surf)} \leftrightarrow MO^{-}_{(surf)} + H^{+}_{(aq)} \quad (2.12)$$

$$MOH_{(surf)} + H^{+}_{(aq)} \leftrightarrow MOH^{+}_{2\ (surf)} \quad (2.13)$$

When the oxide solid in an aqueous solution stays in equilibrium, a hydroxylated surface should be generated. Subsequent dissociation of hydroxyls at the given pH, generates the surface charge, and the level of H^+ and OH^- concentration determines the surface potential (Yopps and Fuerstenau, 1964).

A different mechanism have been postulated by Parks and Bruyn (1962) to explain surface charge generation on oxide minerals. They suggest that oxide minerals are partially dissolved in solution and hydroxyl complexes are generated (Equation 2.14). While hydroxyl metal complex successively adsorb on the surface of oxide minerals, surface charge are generated (Equations 2.15 and 2.16).

$$M_2O_{3_{(solid)}} + 3H_2O \leftrightarrow 2M(OH)_{3_{(aq)}} \quad (2.14)$$

$$M(OH)_{3_{(aq)}} \leftrightarrow M(OH)^{3-m}_{m\ (aq)} + (3-m)OH^{-}_{(aq)} \quad (2.15)$$

$$M(OH)_m^{3-m}{}_{(aq)} \leftrightarrow M(OH)_m^{3-m}{}_{(surf)} \quad (2.16)$$

Two types of mechanisms are suggested to explain how a surface charge is generated, either of which would cause the same degree of pH change in the suspension.

When oxide minerals such as hematite are in aqueous solution, hydroxylated surfaces are generated. Subsequently, surface charge arises depending on pH when hydroxyls dissociate from the surface as expressed in Equations 2.17 and 2.18 (Rao, 2004).

$$Fe(OH)_{3(solid)} + H^+ \leftrightarrow Fe(OH)_2^+ + H_2O \quad (2.17)$$

$$Fe(OH)_{3(solid)} \leftrightarrow FeO_2^- + H^+ + H_2O \quad (2.18)$$

The surface charge is governed by the adsorption of potential-determining ions. When potential determining ions are H^+ and OH^-, the surface charge (σ_s) on a mineral in aqueous solution is given in Equation 2.19.

$$\sigma_s = F(\Gamma_{H^+} - \Gamma_{OH^-}) \quad (2.19)$$

In Equation 2.19, F is the Faraday constant, Γ_{H^+} is the adsorption density in moles per square centimeter of H^+, and Γ_{OH^-} is that of the OH^- ions (Fuerstenau and Raghavan, 2007).

2.4.3 Point of Zero Charge and Isoelectric Point

The Equations 2.12 to 2.19 show that the surface is positively charged when hydrogen ion binds to the hydroxylated surface or hydroxyl ion separates from the surface. A negative surface is produced by the removal of a hydrogen ion from the hydroxylated surface or the binding of a hydroxyl ion to the surface. At a certain pH the numbers of positive sites and negative sites at the surface make equal, leading to the uncharged surface in the solution. When this occurs, the activity of potential determining ions is called the point of zero charge, or PZC, which is the most important factor presenting the surface conditions (Fuerstenau and Raghavan, 2007).

In the case of most minerals, including oxide minerals, the PZC is presented in pH scale because their potential determining ions are H^+ and OH^-. Some examples of PZC of oxide minerals are presented in Table 1. For example, the PZC of synthetic hematite is pH 8.6, which implies that there exist excess OH^- ions on the synthetic hematite surface at pH higher than 8.6. Therefore the surface of the hematite has negative potential at pH above 8.6. Likewise, at pH lower than 8.6 the excessive H^+ ions lead to positive potential at the surface. The adsorption densities of H^+ and OH^- ions are balanced at pH 8.6, hence the potential equals to zero. Since the values in the table are typical results, however, some variations could be observed depending on the source of oxide with difference of impurities and method of pre-treatment (Fuerstenau and Raghavan, 2007).

Table 1: PZC of some oxides (table from Fuerstenau and Raghavan (2007), and data originally from (Fuerstenau, 1970))

Material	PZC, pH
SiO_2, silica gel	1-2
SiO_2, α-quartz	2-3
Fe_2O_3, hematite (natural)	4.8-6.7
Fe_2O_3, hematite (synthetic)	8.6
FeOOH, goethite	6.8
SnO_2, cassiterite	4.5
ZrO_2, zirconia	4
TiO_2, rutile	5.8-6.7
Al_2O_3, corundum	9.1
AlOOH, boehmite	7.8-8.8
MgO, magnesia	12

Isoelectric point (IEP) is often used interchangeably with PZC when there is no specific adsorption of ions except for potential determining ions. IEP indicate the pH of suspension when the zeta potential of solids is zero. The measurements of IEP is conducted by electrophoresis or electroacoustics whereas PZC is obtained from the adsorption density of potential-determining ions as a function of pH and ionic strength using indifferent electrolytes. Table 2 presents the PZC and IEP of iron oxides, and generally both measurements are located at the similar pH range. There could be slight difference between them due to the varying origin and mineralogy, experimental procedure, and aging at suspension (Rao and Forssberg, 2007).

Table 2: PZC, and IEP of the iron oxides (table from Rao and Forssberg (2007), and data originally from Cornell and Schwertmann (1996), Fuerstenau and Palmer (1976), Parks (1965), and Parks and Bruyn (1962))

Oxide	PZC, pH	IEP
Goethite	7.5	6.1, 6.7, 5.9-7.2
	8.9	
	9.2	
Hematite	7.8	5.0, 6.0, 6.7, 8.2, 8.5
	9.5	
	8.5	
Magnetite	7.1	6.5
	6.4	
	6.3	
Maghemite	6.6	6.6

2.5 Flotation of Iron Oxide

Most iron ores come from oxide, and the important iron minerals are magnetite (Fe_3O_4), hematite (Fe_2O_3), and goethite ($Fe_2O_3H_2O$) with the gangue being primarily silica (SiO_2), alumina (Al_2O_3), lime (CaO), sulfur, and phosphorus. To meet the requirements from the blast furnace the iron ores are processed through crushing/grinding, washing/dewatering, sizing, gravity/magnetic concentration, flotation, and pelletizing/sintering. The feeds for flotation comes from magnetic separation, and flotation removes silica and phosphorous impurities, then upgraded final products are achieved (Rao and Forssberg, 2007).

Among nonsulfide minerals, the characteristics of iron oxide is differentiated from the groups of soluble salt or semisoluble salts, so iron oxide is usually subcategorized as a group of "insoluble oxide and silicate" minerals. For the iron oxide flotation in general, as well as silicate minerals, the relation between flotation results and variation of pH showed good correlation with the electrical properties of the particle surfaces. Anionic collectors float the oxide minerals at lower pH than their PZC, and cationic collectors float them at a pH region higher than the PZC of the mineral. With the similar PZCs of goethite, hematite, and magnetite, their flotation results with anionic and cationic collectors are closely comparable (Rao and Forssberg, 2007). More details will be reviewed at Section 2.5.1 for goethite, and at Section 2.5.4 for hematite and magnetite.

The major factors to consider for iron oxide flotation are electrical properties of surface, ionic strength of collector, molecular weight of collector, and solubility of minerals (Rao, 2004). The factors affect the mechanism of collector adsorption, therefore physical adsorption, chemisorption, and surface reaction/precipitation occurs respectively depending on the conditions in the flotation pulp. Physical adsorption is the most popular mechanism in oxide mineral flotation.

2.5.1 Physical Adsorption on Iron Oxide

Electrostatic interaction is main mechanism for many collectors which adsorb on the surface of oxide and silicate minerals. Simple information of PZC values of minerals can help successful use of those collectors. Figure 6 presents the studies of Iwasaki *et al.* (1960b), which showed that the effect of electrostatic phenomena determines recovery of goethite. When dodecyl sulfate and dodecyl sulfonate collectors are used for goethite flotation, high recovery is achieved at the pH lower than PZC of goethite (pH 6.7). The surface of goethite is positively charged at pH lower than PZC, therefore anionic sulfonate ions are adsorbed on the surface, and flotation results. When dodecyl amine was used, goethite is floated at pH above 6.7. Above the PZC of goethite, cationic amine heads are adsorbed on the negatively charged surface, and the successful recovery occurs.

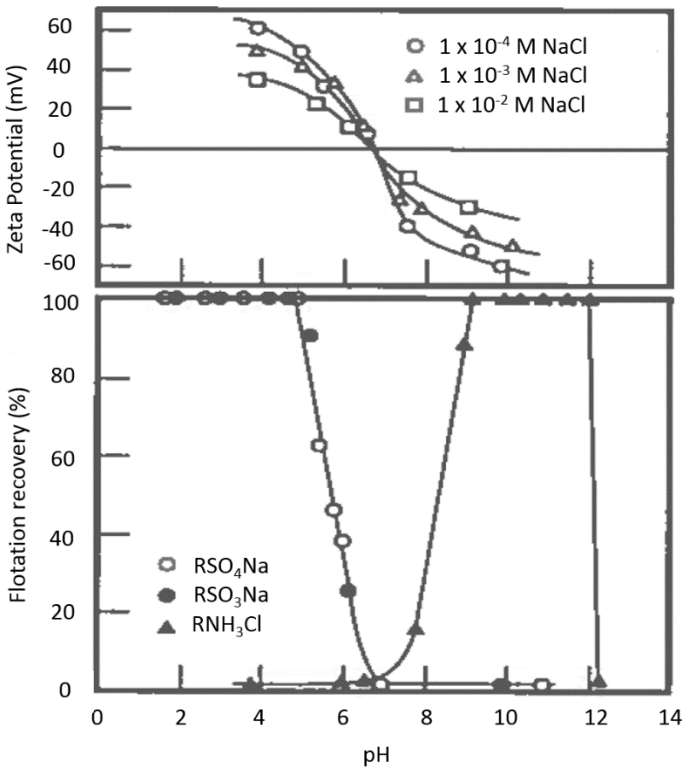

Figure 6. Dependence of goethite flotation on surface charge (chart from Rao and Forssberg (2007), and data originally from Iwasaki *et al.* (1960b))

Fuerstenau *et al.* (1964) studied the effect of hydrocarbon chain length on flotation, and found that more effective recovery is associated with higher collector concentration and longer hydrocarbon chain length, hence supporting the necessary formation of hemimicelles or precipitates of collectors. They also showed that the formation of hemimicelles or precipitate of collector and subsequent removal of hydrocarbon chains from solution decrease the free-energy. Figure 7 describes how the electrical double layer organises adsorbed surfactants. The generation of hemimicelles or precipitation of surfactant molecules is dependent on the relative

concentrations of surfactant. If the required concentration for generating hemimicelles is lower than that for precipitating the surfactant, the formation of hemimicelles would prevail in the suspension (Fuerstenau, 2007).

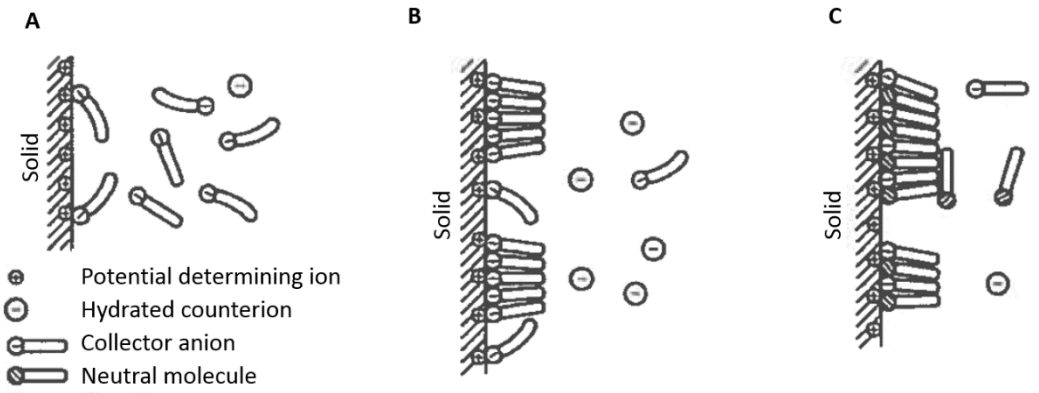

Figure 7. Illustrative interactions of surface-active organic compounds at the electrical double layer (figures from Fuerstenau (2007), and original source from Aplan and Fuerstenau (1962)): (a) single ions of surfactant adsorbed at low concentration of collectors, (b) hemimicelles of collectors formed at higher concentration, and (c) ions and neutral molecules of collectors co-adsorbed

2.5.2 Chemisorption and Surface Reaction/Precipitation on Oxide Minerals

In oxide mineral flotation, the application of chemisorption is not as common as flotation by physical adsorption of surfactants. For chemisorption flotation, Fuerstenau *et al.* (1970) utilized strong chemisorption bonds between hematite and a hydroxamate for hematite flotation, and Bogdanov *et al.* (1973) utilized a chemisorbing hydroxamate for the flotation of huebnerite (Fuerstenau, 2007).

Reaction or precipitation at the surface of oxide and silicates require movement of metallic atoms when interacting with surfactants, and those phenomena are distinguished from physical adsorption or chemisorption. When collectors of high molecular weight are involved, ions from oxides and silicates found to experience hydrolysis, and these reactions are utilized in flotation of pyrolusite with oleate at pH 9 (Fuerstenau and Rice, 1968), and chromite with oleate at pH 9 and pH 11 (Palmer *et al.*, 1975).

2.5.3 Reagents for Iron Oxide Flotation

For iron oxide flotation, mostly non-thio, ionisable surfactants are used, such as anionic fatty acids (particularly oleic acid), alkyl sulfates, or alkyl sulfonates. The iron oxides are separated from silicate gangue in direct flotation using anionic collectors, and silicates are floated from iron oxides in reverse flotation using

cationic collectors. The common cationic surfactants used are alkyl amines, alkyl amine salts, ether amines, and diamines.

The alkyl sulfates and alkyl sulfonate collectors remain ionized across the flotation pH range, and act as strong electrolytes. The alkyl carboxylic acids and hydroxamic acids are weak acids, and alkyl amines or diamines are weakly basic. Those weak acidic or basic surfactants have their predominant ionic or molecular species depending on the pH, hence their dissociation constants are of significant importance. If the surfactants are in a pH range which is over their solubility limit, the molecular species of the surfactants predominate. In case of fatty acid and amines they resulted in a typical colloidal phase at the pH over their solubility limits. In more detail, 0.02 mM oleic acid is ionized as $R(COO)^-$ and $R(COO)_2^{2-}$ at high pH values (> pH 8), and remains as neutral molecules at lower pH. In the mid-pH range the ionomolecular complex is formed as $(RCOO)_2H^-$ (Ananthapadmanabhan and Somasundaran, 1988). In the case of dodecyl amine, it exists as ionized forms of RNH^{3+} in neutral and acidic pH regions but as molecules in very alkali solutions (Rao and Forssberg, 2007). Similarly, an alkyl sulfate of sodium dodecyl sulfate (SDS) is completely disassociated at pH > 3. At pH < 3, an alcohol and a bisulfate are formed due to hydrolysis of sulfate. In case of cetrimonium bromide, or hexadecyltrimethyl-ammonium bromide (HTAB), which is quaternary ammonium salts used as cationic surfactants, it remains disassociated stably in both acidic and alkaline solution (Rao, 2004).

Sodium silicate is widely employed to disperse silicate gangue minerals, and their interaction is dependent on the concentration and pH of the pulp (Rao and Forssberg, 2007; Sjoberg and Ohman, 1985). Starches are used for depressing iron oxides when floating silica and silicates in reverse flotation. They are also employed for flocculating fine iron minerals (Sresty and Somasundaran, 1980).

2.5.4 Direct Flotation of Iron Oxide Ore

Selective flotation of iron oxides from silicate gangue is direct flotation. In contrast, reverse flotation describes flotation of silicates from iron oxides. When selectively separating iron oxide from silicates by flotation the difference in the PZC of the constituting minerals is the most relevant factor for the high selectivity.

Figure 8 (a) shows the complete recovery of hematite with sodium dodecylsulfate (SDS) at a pH lower than the PZC of hematite (pH 6.7). On the other hand, hematite is not recovered at pH greater than the PZC. The use of cationic dodecyl ammonium chloride (DACl) for the direct flotation of hematite leads to successful recovery only at the pH greater than 6.7. At the same condition, the recovery of quartz also occurs (Figure 8 (a)).

The PZC of magnetite (pH 6.5) is comparable with that of hematite, thus the flotation response of magnetite showed similar results to that of hematite when SDS and DACl are used, respectively. Once again, the successful separation of iron oxide minerals are mainly affected by the differences in the PZC of the minerals.

Therefore, if additional silicate gangue mineral, of which the PZC is located between that of silica and magnetite, is introduced to the system, it would be difficult to obtain a separation through flotation. Cummingtonite ($Fe_2Mg_5Si_8O_{22}(OH)_2$) is a metamorphic amphibole and a silicate gangue mineral often found in magnetite iron ores. As PZC of cummingtonite is located between silica and magnetite, shown in Figure 8 (b), highly selective flotation is discouraged.

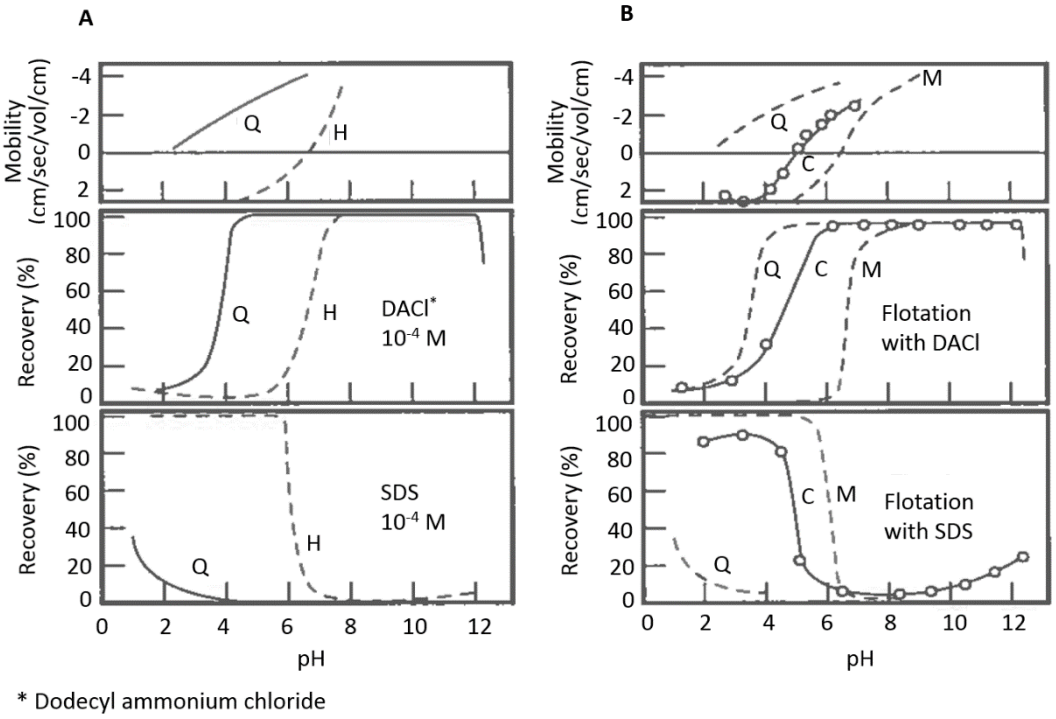

Figure 8. Electrophoretic mobility and flotation results: (a) hematite (H) and quartz (Q), (b) magnetite (M), cummingtonite (C), and quartz (Q) (chart from Rao and Forssberg (2007), and data originally from Iwasaki, (1983), Iwasaki *et al.* (1960a), and (1961))

2.5.5 Reverse Flotation of Iron Oxide Ore

The primary long-chain alkylammonium salts are widely used for the cationic flotation of separating silicate minerals, and the use of which was studied extensively (Fuerstenau and Raghavan, 1978; Fuerstenau, 1995; Smith and L Scott, 1990). The ether amines and diamines are adopted for the removal of silicates from iron oxide ore, and diamines are known as more effective than monoamines for flotation (Rao and Forssberg, 2007).

The mechanism of amine adsorption on silicates is dependent on the pH of the suspension. Cationic amine ions are postulated to adsorb on the negatively charged silicates surface by electrostatic interaction at pH > 2. As the amine concentration increases, the formation of two-dimensional amine aggregates occur in association with their hydrophobic tails, which are called hemimicelles. Therefore the strong hydrophobic forces are introduced by amine hemimicelles, which lead to successful flotation of silicates (Chernyshova *et al.*, 2000, 2001).

Although the opposite surface charges of quartz and hematite are favorable for the removal of silicate by amine flotation, the two minerals pose opposite charges only in a narrow pH range. This phenomena is related to amine adsorption on both minerals, which resulted in poor selectivity. However the addition of starches or dextrins were found to depress the flotation of iron oxide when silica is floated with amine collectors. Amongst a variety of starches and their derivatives, a corn starch,

which is prepared with the least alteration, showed higher depressing ability than other starch derivatives (Chang, 1954). Montes-Sotomayor *et al.* (1998) studied the specific adsorption of starch on hematite by means of observing an IEP shift of hematite, and found that starch adsorbed on hematite and quartz but desorbed from quartz in alkaline conditions with amine collector usage, leading to selective quartz flotation by amine collectors in alkaline media.

3 Experimental Methodology

3.1 Materials

Samples of synthetic iron (III) oxide (Fe_2O_3) and silicon dioxide (SiO_2) were purchased from Sigma-Aldrich, and used for experiments on synthetic minerals. Hematite concentrate from Fire Lake Mine (Quebec, Canada) and natural quartz purchased from VWR were prepared for the experiments with natural minerals. Table 3 details the size, density and specific surface area of the samples used. The particle-size distributions of the samples were examined by laser scattering (Horiba,LA-920, Japan), and the surface areas were calculated by the Barrett-Emmett-Teller(BET) method using a Tristar 3000 (Particle and Surface Sciences, Australia).

Table 3: Characteristics of the particles used in the study

Sample Notation	Minerals (chemical formula)	Density g/cm^3	Particle size d_{50} µm	BET m^2/g
Fe_2O_3	Synthetic Iron (III) oxide (Fe_2O_3)	5.1	0.9	5.4
SiO_2	Synthetic Silicon dioxide (SiO_2)	2.7	2.3	6.2
Hematite	Hematite (Fe_2O_3)	5.0	2.7	1.7
Quartz	Quartz (SiO_2)	2.7	6.7	1.3

According to manufacturers' information, the purity of iron (III) oxide and silicon dioxide were 99% or higher for Fe_2O_3 and SiO_2, respectively. Hematite concentrate included 95.1% iron (III) oxide contents according to acid digestion results, and quartz sample has 99.7% silicon dioxide contents according to the information from the vendor. The detailed procedure about acid digestion is presented in Section 3.6.

The anionic surfactant sodium dodecylsulfate (SDS) and the cationic surfactant hexadecyltrimethylammonium bromide (HTAB) were purchased from Fisher Scientific and Sigma-Aldrich, respectively. The purity of the anionic and cationic surfactants were > 99%, and > 96%, respectively, therefore used without further purification. Potassium chloride (KCl) was purchased from Sigma-Aldrich and used to provide background electrolyte. The water used was processed with reverse osmosis (Barnstead Thermo Scientific, D12671, United States).

In order to achieve consistent dispersions of minerals, the suspensions underwent ultrasonication (Hielscher Ultrasonics, UP400S, Germany). The concentrations of the suspensions were 3% w/w with 10^{-3} M KCl background electrolyte for the zeta potential measurements, and 10% w/w for CGA flotation. The electrolyte solution ensured constant ionic strength for the zeta potential measurements. These conditions were kept constant for all experiments.

3.2 Determination of Critical Micelle Concentration

The critical micelle concentration (CMC) of each surfactant (SDS and HTAB) was determined by measuring the change of surface tension as a function of concentration. Seven different levels of concentrations were used for SDS (0.5, 1.0, 1.5, 2.0, 2.5, 3.0, and 4.0 g/l) and HTAB (0.1, 0.2, 0.25, 0.3, 0.5, 1.0, and 2.0 g/l), and surface tensions of the surfactant solutions were measured by the Wilhelmy plate method (Krüss GmbH, K12, Germany). Each series of experiments are termed Experiment A-1, and Experiment A-2 for SDS and HTAB, respectively, and details are summarized in Table 4. Tests were done in quintuplicates, and results are presented in Figure 11.

Table 4: List of surface tension measurement experiments

Experiment notation	Materials	Concentrate (g/l)	Results
A-1	SDS solution	0.5, 1.0, 1.5, 2.0, 2.5, 3.0, and 4.0	Fig. 11
A-2	HTAB solution	0.1, 0.2, 0.25, 0.3, 0.5, 1.0, and 2.0	Fig. 11

3.3 Half Life and Gas Holdup of Microbubbles

An acrylic vessel equipped with 4 baffles was prepared for the measurement of half life and gas holdup of CGA. For the CGA generation, 100 ml of surfactant solution was stirred using a high speed mixer (Troemner LLC, Talboy 101, USA). In the vessel, a disc impeller rotated at 7,000 rpm. For the design and modification of the apparatus, the works by Save and Pangarkar (1994) were adopted. The schematic of the apparatus is shown in Figure 9.

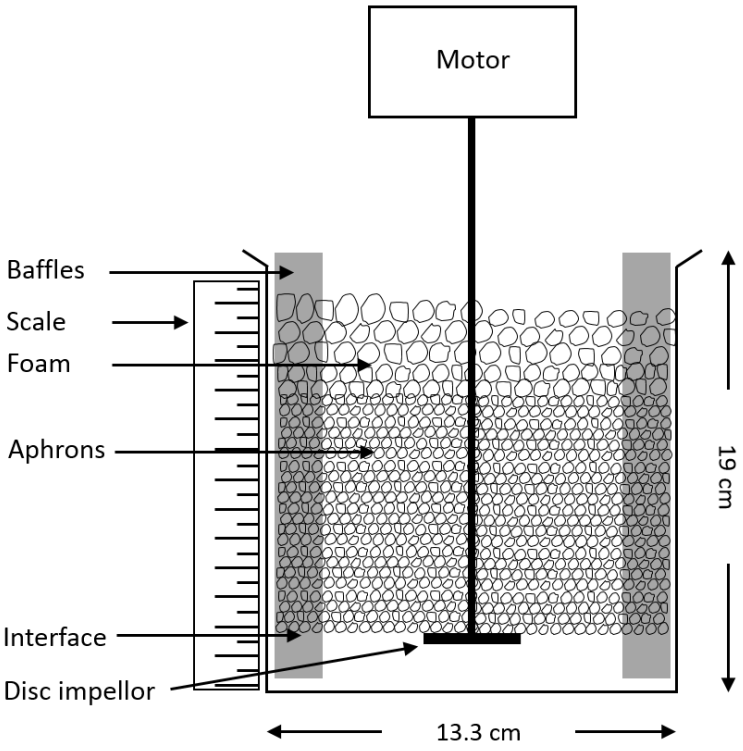

Figure 9. Experimental set up for half life and gas holdup measurement, adapted from Save and Pangarkar, (1994)

Surfactant concentration, electrolyte concentration, and pH are considered to be major parameters related to the stability of CGA. Previous research generally agrees that increasing surfactant concentration increases the stability (Feng *et al.*, 2009; Jarudilokkul *et al.*, 2004; Jauregi *et al.*, 1997) and higher levels of electrolyte are detrimental to the stability because of the depression of double layers. Jauregi *et al.* (1997), and Save and Pangarkar (1994) reported no significant pH effect on the stability, but Feng *et al.* (2009) reported decreasing CGA stability with increasing pH (Jauregi and Dermiki, 2010), therefore the effect of pH on the stability of CGA is not conclusive yet. In this project, the characteristics of CGA were tested at natural pH without background electrolyte, therefore surfactant concentration was considered as the only parameter to test CGA stability. Those experiments are named Experiments B-1 to B-4, and Table 5 summarizes the experiments.

Table 5: List of half life and gas holdup measurement experiments

Experiment notation	Measurement	Materials	Results
B-1	Half life	SDS CGA	Fig. 12
B-2	Gas holdup	SDS CGA	Fig. 12
B-3	Half life	HTAB CGA	Fig. 13
B-4	Gas holdup	HTAB CGA	Fig. 13

3.4 Recovery of Fine Particles with CGA Flotation System

To verify the interactions between fine particles and CGA, flotation experiments were conducted with single mineral feeds. An 8 litre baffled vessel was used for the generation of CGA dispersions. The flotation column had dimensions of 9 cm diameter and 23 cm height. It was filled with a suspension composed of 180 ml of water and 20 g of mineral, giving an initial solids contents of 10% by weight. A schematic of the CGA flotation system is shown in Figure 10.

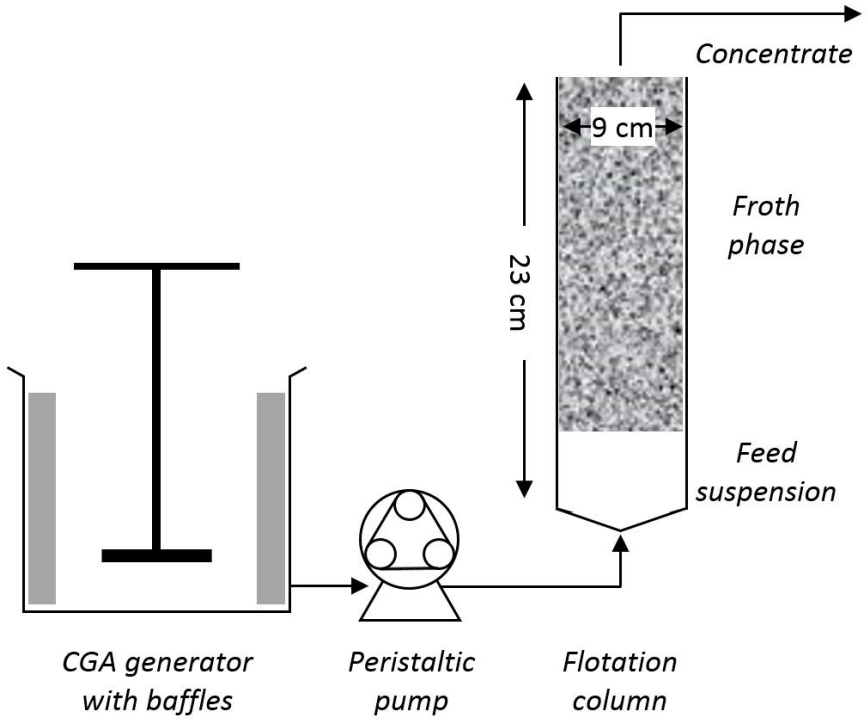

Figure 10. Schematic of the CGA flotation column system, adapted from Waters *et al.* (2008)

The CGA dispersion from the generator was pumped into the bottom of the flotation column, rising through the suspension to form froth, and making up concentrate. The initial height of the feed suspension was 2 cm, where 0 cm is considered to be the lowest point at which the column is at its full diameter. While CGA were pumped to the column by peristaltic pump (Cole-Parmer Instrument Co., Masterflex 7520-25 and Easy-load 7518-00, USA) for 11 minnutes, the froth reached the lip of the column after 6 min in average with variations depending on the experiment. The overflow was recovered until the CGA supply was exhausted, after which the froth phase was collected by suction (Cole-Parmer Instrument Co., Aspirator pump 7050-00, USA). The recovered overflow and froth were dried in an oven, and particles were collected. Over the course of the experiment, the pulp-froth interface rises because CGA dispersion is provided continuously into the column. Therefore, the amount of surfactant in the system also keeps increasing until each experiment is over. Tests were conducted for eight sets of experiments (① Fe_2O_3-SDS CGA, ② SiO_2-SDS CGA, ③ Fe_2O_3-HTAB CGA, ④ SiO_2-HTAB CGA, ⑤ hematite-SDS CGA, ⑥ quartz-SDS CGA, ⑦ hematite-HTAB CGA, and ⑧ quartz-HTAB CGA) in either triplicate or quintuplicate, and details are summarized in Table 6 for the experiments with synthetic materials and in Table 7 for those with natural minerals.

Table 6: List of recovery experiments with synthetic minerals

Experiment notation	Flotation Media	pH	Feed (w/w)	Results
C-1	SDS CGA	3, 5, 7, 8, 10	Fe_2O_3 10%	Fig. 15
C-2	SDS CGA	3, 5, 7, 8, 10	SiO_2 10%	Fig. 16
C-3	HTAB CGA	3, 5, 7, 8, 10	Fe_2O_3 10%	Fig. 19
C-4	HTAB CGA	3, 5, 7, 8, 10	SiO_2 10%	Fig. 20

Table 7: List of recovery experiments with natural minerals

Experiment notation	Flotation Media	pH	Feed (w/w)	Results
D-1	SDS CGA	3, 5, 7, 10	Hematite 10%	Fig. 25
D-2	SDS CGA	3, 5, 7, 10	Quartz 10%	Fig. 26
D-3	HTAB CGA	3, 5, 7, 10	Hematite 10%	Fig. 27
D-4	HTAB CGA	3, 5, 7, 10	Quartz 10%	Fig. 28

3.5 Zeta Potential Measurements

Electroacoustic measurements were conducted using the Field ESA (Partikel-Analytik-Messgeräte, Germany), which equipped with Titrator PA 100 (Partikel-Analytik-Messgeräte, Germany). Prior to each set of experiment, the suspensions were allowed 30 minutes to reach equilibrium. The effect of pH on the zeta potential was determined by titrating the suspension from the natural pH to the range between pH 3 and pH 10 by 0.5 pH steps. Acid and base was added (1 M HCl and 1M NaOH, respectively), and the suspension was allowed 5 minutes to reach equilibrium for the each pH step. In this project, the experiments are termed as Experiments E-1 and E-2 for synthetic materials and as Experiments F-1 and F-2 for natural minerals. The summary of zeta potential measurement experiments are presented in Table 8 and Table 9.

Table 8: List of zeta potential measurement experiments with synthetic minerals

Experiment notation	Media	Suspension (w/w)	pH	Results
E-1	KCl (10^{-3} M)	Fe_2O_3 3%	3~10	Fig. 14
E-2	KCl (10^{-3} M)	SiO_2 3%	3~10	Fig. 14
E-3	KCl (10^{-3} M) + SDS additions	Fe_2O_3 3%	3~10	Fig. 17
E-4	KCl (10^{-3} M) + SDS additions	SiO_2 3%	3~10	Fig. 18
E-5	KCl (10^{-3} M) + HTAB additions	Fe_2O_3 3%	3~10	Fig. 19
E-6	KCl (10^{-3} M) + HTAB additions	SiO_2 3%	3~10	Fig. 20
E-7	KCl (10^{-3} M)	Fe_2O_3 10%	3~10	Appendix 1
E-8	KCl (10^{-3} M)	SiO_2 10%	3~10	Appendix 2

Table 9: List of zeta potential measurement experiments with natural minerals

Experiment notation	Media	Suspension (w/w)	pH	Results
F-1	KCl (10^{-3} M)	Hematite 3%	3~10	Fig. 24
F-2	KCl (10^{-3} M)	Quartz 3%	3~10	Fig. 24
F-3	KCl (10^{-3} M) + SDS additions	Hematite 3%	3~10	Fig. 25
F-4	KCl (10^{-3} M) + SDS additions	Quartz 3%	3~10	Fig. 26
F-5	KCl (10^{-3} M) + HTAB additions	Hematite 3%	3~10	Fig. 27
F-6	KCl (10^{-3} M) + HTAB additions	Quartz 3%	3~10	Fig. 28
F-7	KCl (10^{-3} M)	Hematite 10%	3~10	Appendix 3
F-8	KCl (10^{-3} M)	Quartz 10%	3~10	Appendix 4

The effect of anionic and cationic surfactant on the zeta potential was investigated by concentration titration and pH titration. SDS solution of 40 g/l was prepared and added to the mineral suspension in 0.2 ml increments at natural pH. For adsorption and equilibrium to be reached, 10 minutes were allowed for every increment of surfactant addition. After the concentration titration curve was obtained, three points of SDS addition amounts were chosen for further analysis. Three sets of suspension were newly prepared and conditioned with the three levels of SDS addition, and pH titrations were conducted with the conditioned suspensions. To measure the effect of cationic surfactants, same experimental procedures were followed with 10 g/l solutions of HTAB. In addition, the zeta potential of 10% w/w suspensions were measured and compared with the results of 3% w/w suspensions. All zeta potential measurements were done in quintuplicate. The experiments are termed as Experiments E-3 to E-8 for synthetic materials and as Experiments F-3 and F-8 for natural minerals as summarized in Table 8 and Table 9.

The effect of solid concentration on zeta potential measurement was studied between suspensions of 3% w/w and 10% w/w solid contents. As presented in Appendix, both types of suspensions did not show any important deviations to each other when their zeta potentials were compared. Therefore this analysis provided reasonable basis of utilizing zeta potential measurements with 3% w/w suspensions for the interpretation of flotation results with 10% w/w suspensions.

Both surfactants used in this projects are known to remain ionized between pH 3 and pH 10. As reviewed in Section 2.5.3, the anionic SDS and cationic HTAB belong to the species of non-thio surfactants with a mono polar group, and this group of surfactants is known to be prone to dissociation, ionization, and hydrolysis, the extent of which is governed by the pH of aqueous solutions. Among them, alkyl sulfates, one of which is SDS, are completely dissociated above pH 3; below this pH, hydrolysis of sulfate progressively takes place with the formation of an alcohol and a bisulfate. Quaternary ammonium salts, to which HTAB belongs, are stable in both acid and alkaline media and completely dissociated (Rao, 2004). Therefore, the chances of deviating properties of SDS and HTAB in the course of experiments were not considered when the experimental results were analyzed.

3.6 Separation of Binary Fine Minerals by CGA Flotation System

Separation experiments were conducted using identical set ups to those used for the single mineral recovery experiments. Suspensions were prepared with 180 ml of filtered water, and 20 g of mineral mixtures (10 g of Fe_2O_3 and 10 g of SiO_2 for the separation of synthetic mineral mixtures, and 10 g of hematite and 10 g of quartz for the natural orebody mixtures). The experiments are termed as Experiments G-1 and G-2 for synthetic materials and as Experiments H-1 and H-2 for natural minerals as summarized in Table 10 and Table 11.

Table 10: List of separation experiments with synthetic minerals

Experiment notation	Flotation Media	pH	Feed (w/w)	Results
G-1	SDS CGA	3, 7, 10	Fe_2O_3 5% + SiO_2 5%	Fig. 21
G-2	HTAB CGA	3, 7, 10	Fe_2O_3 5% + SiO_2 5%	Fig. 22

Table 11: List of separation experiments with natural minerals

Experiment notation	Flotation Media	pH	Feed (w/w)	Results
H-1	SDS CGA	3, 7, 10	Hematite 5% + Quartz 5%	Fig. 29
H-2	HTAB CGA	3, 7, 10	Hematite 5% + Quartz 5%	Fig. 31

The resulting samples from overflow and froth underwent acid digestion of iron (III) oxide by use of hydrochloric acid (36.5%, Fischer Scientific) and nitric acid (69%, Fischer Scientific), and the iron concentration were determined by fast sequential atomic absorption spectrometer (Varian, Inc., AA240 FS, USA) for the subsequent calculation of grade and recovery.

4 Results and Discussion

4.1 Surface Tensions of Surfactant Solutions

The solutions of seven different concentrations (0.5, 1.0, 1.5, 2.0, 2.5, 3.0, and 4.0 g/l for SDS, and 0.1, 0.2, 0.25, 0.3, 0.5, 1.0, and 2.0 g/l for HTAB) were used for the surface tension measurement (Experiments A-1 and A-2). The CMC was measured to be between 2.0 and 2.5 g/l for SDS (Experiment A-1) as shown in Figure 11, corresponding to the information provided by the manufacturer (CMC at 8.3 mM; equivalent to 2.4 g/l), and, between 0.3 and 0.5 g/l for HTAB (Experiment A-2), which also matched with manufacturer's value (CMC at 0.92 ~ 1.0 mM; equivalent to 0.33 ~ 0.36 g/l).

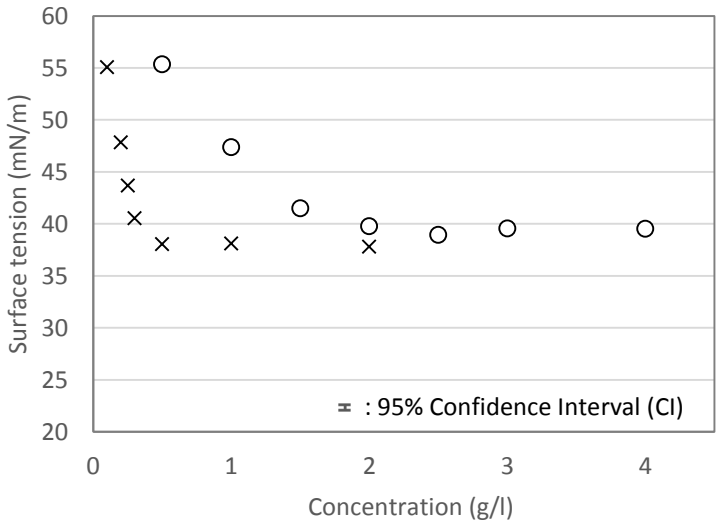

Figure 11. Surface tensions of surfactant solutions (SDS and HTAB): ○, SDS solution; ×, HTAB solution

Confidence interval (CI) was calculated by pooling the variances of measurement with 5% significance level (95% confidence level) assuming that probability of the observed values followed Student's t-distribution. Same method and assumptions were applied to all the CI presentations.

4.2 Half Life and Gas Holdup of CGA

The purpose of characterizing CGA was to decide surfactant concentration for the subsequent flotation. The same concentration of surfactant solutions as those with Experiment A-1 were adopted for the experiment of half life and gas holdup measurement of SDS CGA (Experiments B-1 and B-2). The halflife increased with increasing surfactant concentration, although the increase diminished dramatically after the concentration reached 3 g/l (Experiment B-1). Gas holdup increased as more concentrated surfactants were used, but did not increase further when the concentration was higher than CMC of 2.4 g/l (Experiment B-2) as presented in Figure 12.

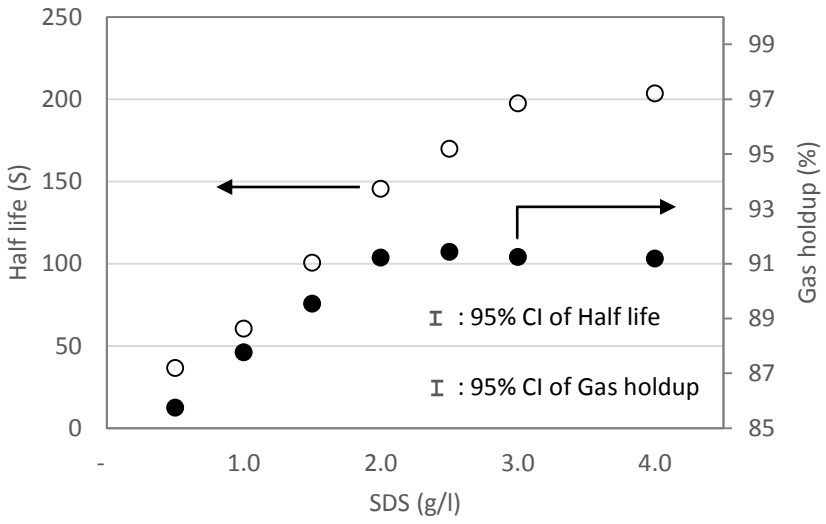

Figure 12. Half life and gas holdup of SDS CGA: ○, Half life; ●, gas holdup

When the same concentration of HTAB solution as Experiment A-2 were used to generate CGA, the change of half life (Experiment B-3) and gas holdup (Experiment B-4) showed similar trends, as shown in Figure 13, to those of the SDS CGA (Experiments B-1 and B-2) in Figure 12.

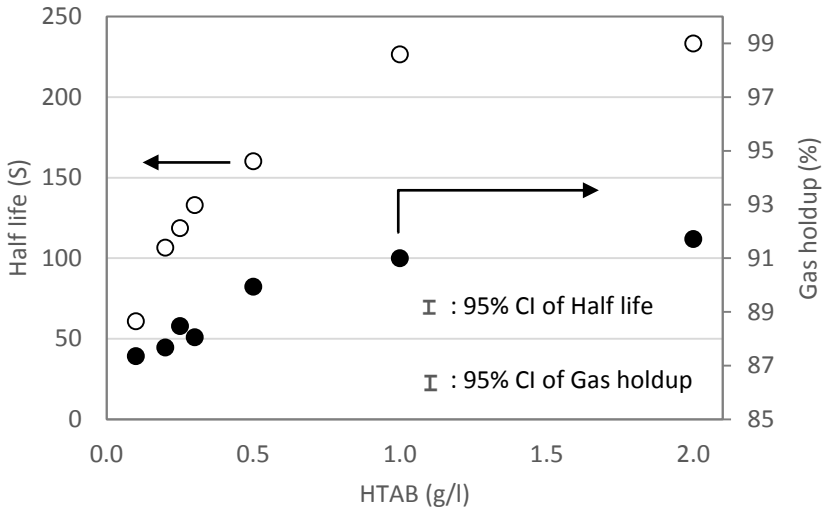

Figure 13. Half life and gas holdup of HTAB CGA: ○, Half life; ●, gas holdup

The increasing concentration of ionic surfactant affects the surface charge and the extent of the electrical double layer, therefore increases repulsive forces between bubbles which oppose film thinning. Therefore a higher concentration of surfactant resulted in a more stable foam (Bhakta and Ruckenstein, 1997). After the characterization of CGA (Experiments B-1 - B-4) and preliminary flotation tests, the half-life of approximately 150 sec was found to provide enough stability as well

as a certain degree of drainage. Therefore the concentration of 2.0 g/l for SDS, and 0.3 g/l for HTAB were chosen for subsequent flotation.

4.3 Synthetic Minerals

4.3.1 Zeta Potential of Fe_2O_3 and SiO_2

The zeta potentials of Fe_2O_3 and SiO_2 were measured (Experiments E-1 and E-2) between pH 3 and 10, and the results are presented in Figure 14.

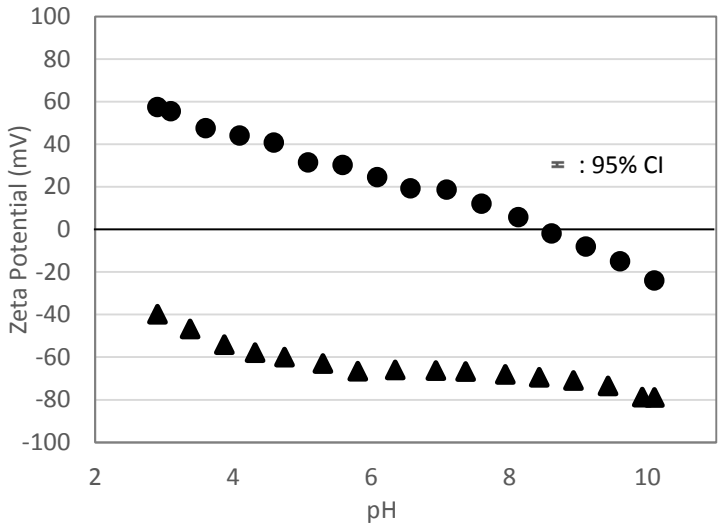

Figure 14. Zeta potential of Fe_2O_3 and SiO_2 as a function of pH: ●, Fe_2O_3; ▲, SiO_2

The natural pH and zeta potential were pH 7.2 and 21 mV for Fe_2O_3 and pH 5.5 and -65 mV for SiO_2. The zeta potential of Fe_2O_3 indicates an IEP of approximately pH 8.5. This corresponds to values quoted by Musić and Wolf (1979), Sposito (2004) and Fuerstenau and Raghavan (2007). Across the pH range investigated, the zeta potential of SiO_2 remained negative. Extrapolation of the curve indicates that the

IEP would occur between the pH 2 and 3, if the trend is indeed followed, and it corresponds to the data quoted by Parks (1965) and Fuerstenau and Raghavan (2007).

4.3.2 Anionic Surfactant (SDS) System

The recovery of Fe_2O_3 by negatively charged SDS CGA (Experiment C-1), and the results of SiO_2 (Experiment C-2) by an identical setup are shown in Figure 15 and 16, respectively.

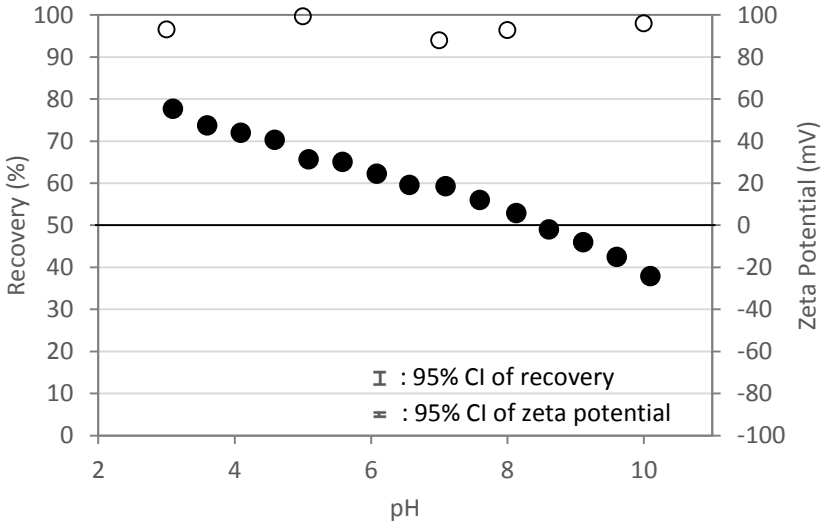

Figure 15. Fe_2O_3 recoveries by SDS CGA flotation as a function of pH, and comparison of Fe_2O_3 zeta potential: ○, Fe_2O_3 recovery; ●, Fe_2O_3 zeta potential

The recovery is the sum of the particles from overflow and froth. The zeta potential results are taken from Experiments E-1 and E-2 for comparison. The recovery of Fe_2O_3 is generally high with minimum 94% recovery across the entire pH range (Experiment C-1).

Conversely, the SiO_2 (Experiment C-2) showed low recoveries with a maximum of 5.7% (Figure 16). Waters *et al.* (2008), and Fuda and Jauregi (2006) observed an important role of electrostatic interactions in the selective attachment of a material onto the surface of CGA. Based upon this, the low recovery of SiO_2 can be interpreted as a result of like charged particles and bubbles repelling each other. However, the supposed repulsive forces between negative charges of Fe_2O_3 and SDS CGA, from the results of Experiment C-1 (Figure 15), does not appear to be very strong at pH 10, with results showing high recoveries of Fe_2O_3. Therefore, it is necessary to develop a detailed understating on how charged CGA interacts with particles.

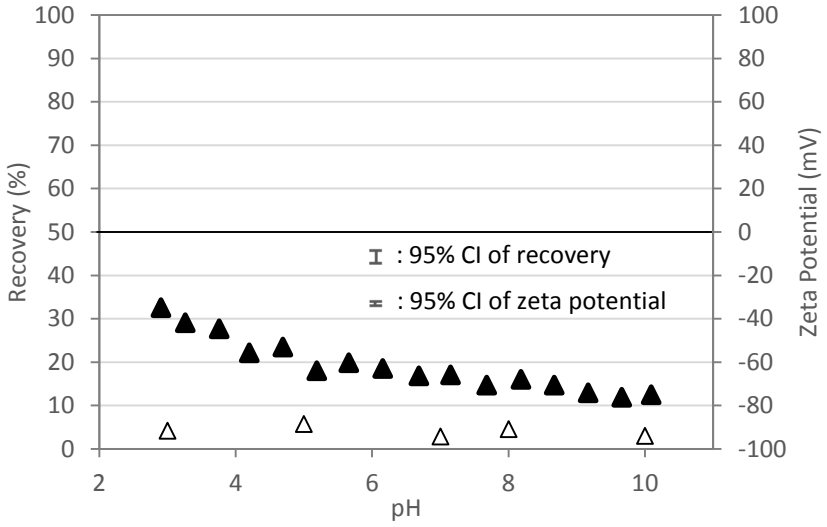

Figure 16. SiO_2 recoveries by SDS CGA flotation as a function of pH, and comparison of SiO_2 zeta potential: △, SiO_2 recovery; ▲, SiO_2 zeta potential

In order to study the interaction between particles and CGA, the indirect method is adopted in this project by correlating the results of two types of experiments. One is to observe interaction between particles and surfactant molecules by means of measuring the change in zeta potentials (Experiments E-3 - E-6, and Experiments F-3 - F-6), and another is to run CGA flotation to recover particles from single mineral feeds (Experiments C-1 - C-4, and Experiments D-1 - D-4). Figure 17 shows the change of Fe_2O_3 zeta potential between pH 3 and pH 10, and the effect of SDS surfactant addition on the zeta potential (Experiments E-1 and E-3).

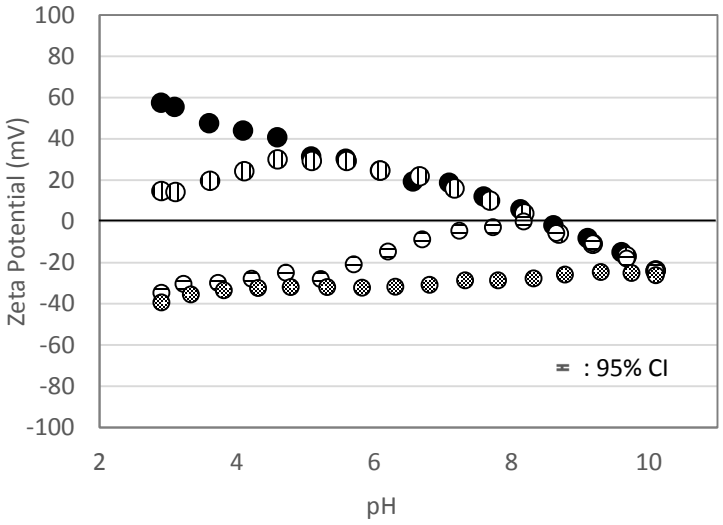

Figure 17. Zeta potential of Fe_2O_3 as a function of pH at different SDS concentrations: ●, Fe_2O_3 only; ◍ 0.4 mg m^{-2} SDS; ⊖ 2.9 mg m^{-2} SDS; ◙, 9.9 mg m^{-2} SDS

SDS surfactant showed high adsorption on the surface of Fe_2O_3 across the entire pH range studied when SDS solution was introduced. Below the IEP, positively charged Fe_2O_3 and the negatively charged sulfonate head of SDS would dominate the adsorption with attractive electrostatic forces. Above the IEP, however, the results showed that negatively charged SDS head adsorbed on Fe_2O_3 particles of negative zeta potentials (Figure 17), which led to the high level of Fe_2O_3 recovery by SDS CGA flotation at pH 10 (Figure 15). This observation could be explained by the previous research by Hankins *et al.* (1996) where the significant adsorption of anionic surfactant above IEP on the surface of an oxide mineral is due to the heterogeneity of the mineral particle's surface, and counterion binding which

stabilize surfactant on the surface. It is the same context with hemimicelles theory as reviewed from Sector 2.5.1. Although the zeta potential of Fe_2O_3 was a negative value at pH 10, the level of negativity was not enough to cover all the positively charged spots of Fe_2O_3 surface, leaving some positively charged areas on which some SDS molecules can adsorb. Therefore SDS hemimicelles could be formed on the surface of Fe_2O_3 with the high concentration of SDS surfactant, leading to sufficient hydrophobic sites for flotation to occur successfully.

The interaction between SiO_2 and SDS is presented at Figure 18 (Experiments E-2 and E-4), and little, if any, evidence of adsorption could be found across the pH range except for pH 3. Johnson *et al.* (2009) used AFM and reported the measurement of a repulsive force when silica glass probe was approached to SDS microbubbles. Accordingly, similar charges from particles and SDS in this experiment are likely to cause repulsive forces between them, which could be the main cause of little SDS adsorption on SiO_2 surface. The lack of interaction found in Experiments E-2 and E-4 (Figure 18) resulted in low recovery of SiO_2 particles when they are floated by SDS CGA (Experiment C-2) as shown in Figure 16. At pH 3, there seems to be some signal of adsorption, but was not sufficient to enhance SiO_2 recovery by SDS CGA.

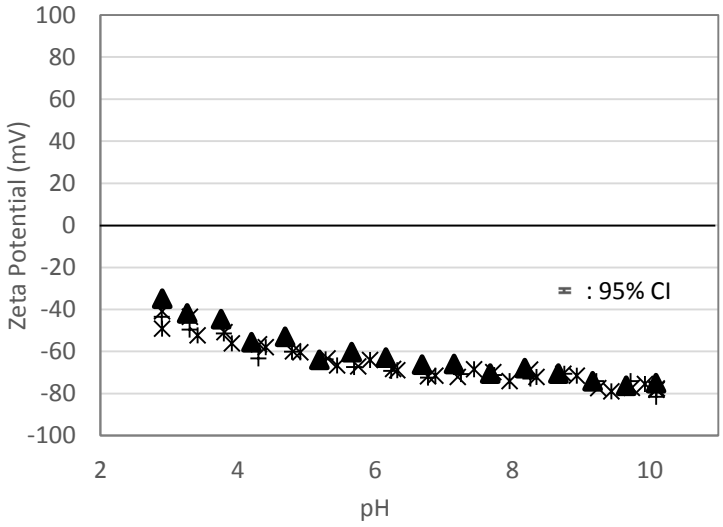

Figure 18. Zeta potential of SiO_2 as a function of pH at different SDS concentrations: ▲, SiO_2 only; × 0.4 mg m^{-2} SDS; ＋ 2.5 mg m^{-2} SDS; ✳, 4.0 mg m^{-2} SDS

A positive correlation was observed based on the qualitative comparison of particle-SDS adsorption (Experiments E-1 - E-4) and particle recovery by SDS CGA flotation (Experiments C-1 and C-2). Sulfonate heads of SDS molecules were electrostatically attracted to the positive spots of Fe_2O_3 surface, and SDS adsorption in Fe_2O_3 particles (Figure 17) was high in all the pH conditions. Thus it resulted in good recovery of Fe_2O_3 between pH 3 and pH 10 (Figure 15). SiO_2 interaction with SDS was rarely observed (Figure 18) due to the repulsive nature of similar charges of them, and this could be related to low recovery presented in Figure 16.

4.3.3 Cationic Surfactant (HTAB) System

In Figure 19, the results of Fe_2O_3 recovery by HTAB CGA flotation (Experiment C-3) are presented and Fe_2O_3 zeta potential measurement at different HTAB concentrations (Experiments E-1 and E-5) are compared. From the result of Experiment C-3 at pH 3 and pH 5, the recoveries were low (from 2.5% to 17.9%). Conversely, when the pH was increased to 10, the recoveries rose to 84.4%, thus the pH dependency of Fe_2O_3 recovery was observed. At pH 3, when the addition of HTAB surfactant was considered (Experiment E-5), little evidence of HTAB adsorption on Fe_2O_3 was observed. Particles of highly positive zeta potential seemed to successfully repel the positively charged amine head of HTAB. There was, however, a strong indication of HTAB adsorption onto Fe_2O_3 at pH 10, and this difference in adsorption led to the different level of Fe_2O_3 recovery at pH 3, and pH 10 (Experiment C-3) as shown in Figure 19. According to the studies by Dobson *et al.* (2000) and Fan *et al.* (1997), the electrostatic interaction is responsible for the initial contact of HTAB ion to the metal surface, and subsequent hydrophobic interactions was found to lead to the hydrophobization by patches of hydrocarbon chains, and the results presented in Figure 19 are in agreement with their studies. From Experiments E-1 and E-5, as pH increases from 3 to 10, the number of negatively charged spots on Fe_2O_3 increases, and more number of HTAB molecules are electrostatically attracted on the surface of Fe_2O_3. This is related to

more interaction between Fe_2O_3 particles and HTAB CGA, therefore, an increased level of recovery was observed as pH increases from 3 to 10 (Experiment C-3).

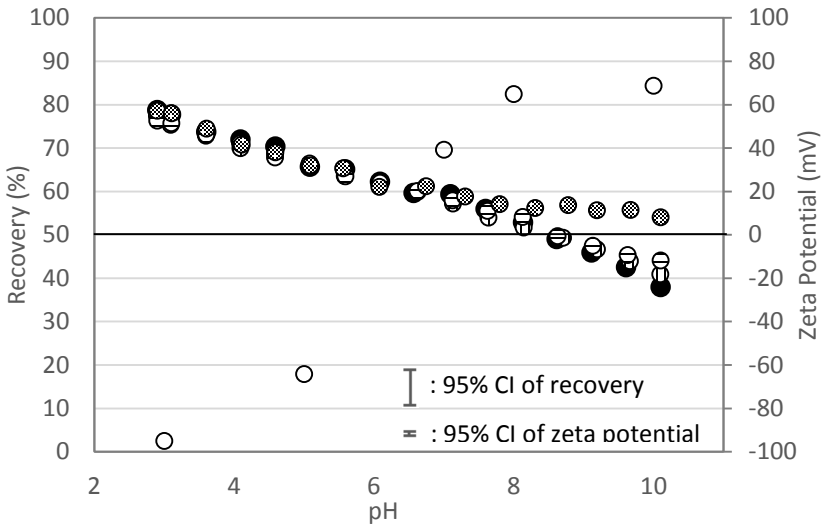

Figure 19. Fe_2O_3 recoveries by HTAB CGA flotation as a function of pH, and comparison of Fe_2O_3 zeta potential at different HTAB concentrations: ○, Fe_2O_3 recovery; ●, Fe_2O_3 zeta potential; ◐, Fe_2O_3 zeta potential with 0.1 mg m^{-2} HTAB; ⊖, Fe_2O_3 zeta potential with 0.4 mg m^{-2} HTAB; ⊜, Fe_2O_3 zeta potential with 0.9 mg m^{-2} HTAB

The results of SiO_2 recovery by HTAB CGA flotation (Experiment C-4) and SiO_2 zeta potential at different HTAB concentrations (Experiments E-2 and E-6) are presented in Figure 20. The SiO_2 recovery by HTAB CGA (Experiment C-4) was high, with minimum recovery of 88.7%, and HTAB showed good adsorption on SiO_2 (Experiment E-6) leading to a charge reversal across the entire pH range. Johnson *et al.* (2009) conducted AFM measurement of interaction between silicon

glass probe and positively charged DTAB (dodecyl trimethylammonium bromide) microbubble, and reported lack of the repulsive forces, which was observed when a silicon glass probe approached SDS microbubble. Similarly, the opposite charges of SiO_2 and the HTAB head would form attractive forces and dominate the adsorption mechanism.

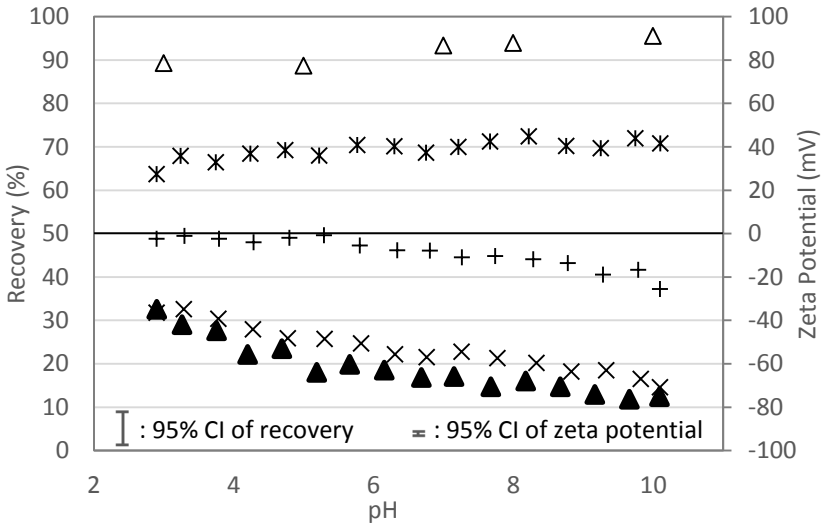

Figure 20. SiO_2 recoveries by HTAB CGA flotation as a function of pH, and comparison of SiO_2 zeta potential at different HTAB concentrations: △, SiO_2 recovery; ▲, SiO_2 zeta potential; ×, SiO_2 zeta potential with 0.1 mg m^{-2} HTAB; +, SiO_2 zeta potential with 0.3 mg m^{-2} HTAB; ✳, SiO_2 zeta potential with 0.8 mg m^{-2} HTAB

HTAB adsorption on Fe_2O_3 (Experiment E-5) showed pH dependency driven by electrostatic characteristics of particles and surfactants, and a similar trend was found in Fe_2O_3 recovery (Experiment C-3) when HTAB derived CGAs were used

to recover particles (Figure 19). When HTAB surfactant was added into SiO_2 suspension (Experiment E-6), the surfactant interaction showed high adsorption across the entire pH range, and it correlated well with the high recovery of SiO_2 by HTAB CGA flotation (Experiment C-4) as presented in Figure 20. When both results of particle-HTAB adsorption (Experiments E-1, E-2, E-5, and E-6) and particle recovery by HTAB CGA flotation (Experiments C-3 and C-4) were compared, it is suggested that particle-HTAB CGA interaction is driven by electrostatic interactions.

4.3.4 Separation of Synthetic Binary Fine Minerals

Separation experiments were conducted with the identical set ups which were used for the recovery of single mineral feeds. By maintaining the same experimental conditions, more reliable comparison could be achieved between the recovery tests with single mineral feed (Experiments C-1 - C-4 for synthetic minerals, and Experiments D-1 - D-4 for natural minerals) and the separation tests of bi-mineral feeds (Experiments G-1 and G-2 for synthetic minerals, and Experiments H-1 and H-2 for natural minerals).

Figure 21 details the separation results of Fe_2O_3-SiO_2 mixture by SDS CGA flotation system with the feed of 50% Fe_2O_3 and 50% SiO_2 (Experiment G-1). From the two markers in each series, left ones represent grade and recovery of overflow, and right markers represent cumulated grade and recovery of overflow and froth. At pH 3, for example, the contents of Fe_2O_3 was 59.5% and 53.6% for overflow and froth, respectively, and they cumulatively resulted in a 55.9% Fe_2O_3 grade of the concentrate.

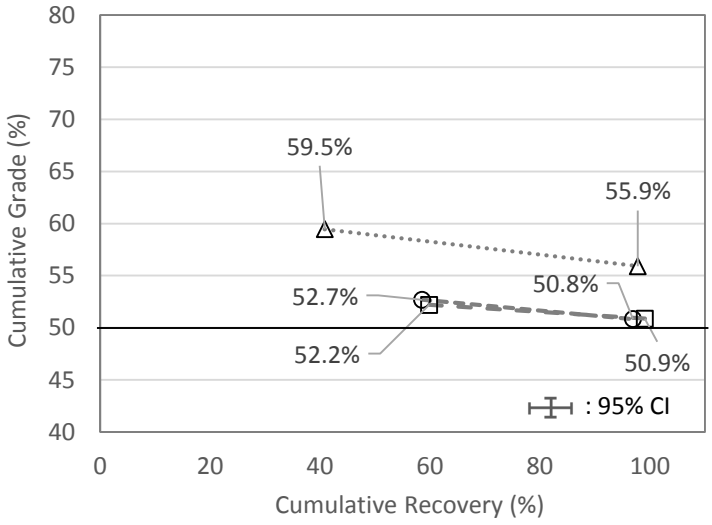

Figure 21. Grade-recovery of Fe_2O_3 by SDS CGA flotation: ···△···, pH 3; - -⊖- -, pH 7; - -⊟- -, pH 10 (data label presents grade, and solid line presents feed grade)

From the negative slopes in Figure 21, it is found that Fe_2O_3 is selectively floated by SDS CGA. If one material is more preferably attached to CGA than another, the grade of the former should be higher with overflow than with froth because the overflow has more time for the drainage of non-selectively entrained minerals than the froth does. Therefore the negative slope of the grade-recovery curve implies that SiO_2 is more readily detached in the drainage process while Fe_2O_3 is retained. The selective attachment of Fe_2O_3 to SDS CGA is in agreements with previous experiments of single mineral recoveries by SDS CGA flotation. As presented in Figure 15 and 16 (Experiments C-1 and C-2), Fe_2O_3 floats but SiO_2 does not float by SDS CGA at all the pH conditions tested. The opposite case of positive slope is

observed with HTAB CGA flotation (Experiment F-2) and will be discussed with Figure 22.

The result of separation at pH 3 shows superior separation results to those from pH 7 and pH 10. What was distinctly observed, while running Experiment G-1 at pH 3, was that there was sediments of white SiO_2 particles from the collected overflows and froth, whereas sediments from other experiments normally showed red color similar to that of Fe_2O_3-SiO_2 mixtures. In more detail from Experiment G-1, the color of sediments gets redder as pH increased from pH 3 to pH 10, and the sediments at pH 10 showed red color, similar to that of Fe_2O_3-SiO_2 mixtures. Among the four categories of separation experiments with Experiments G-1, G-2, H-1, and H-2, such a color variation of sediments were observed only from Experiment G-1.

Considering a large positive zeta potential of Fe_2O_3 at pH 3 (+ 55.4 mV), the supposed dispersed states of Fe_2O_3 particle could possibly be related to the easy drainage of SiO_2 impurities if Fe_2O_3 particles are strongly attached to anionic SDS CGA rather than SiO_2, and if the CGA starts to repel SiO_2 impurities from supposed Fe_2O_3-SiO_2 flocculates. However, due to the limited experimental design for this project, the effect of aggregation and flocculation has not been examined, as such further studies to verify this hypothesis should be undertaken. Although fundamental rationale behind this phenomena is not conclusive yet, it was observed

that SiO_2 is easily separated from Fe_2O_3 at pH 3, therefore more selective separation was achieved.

For this project, every element of overflow or froth, respectively, was treated as one subject, therefore subsequent sedimentation was not considered separately. If there could be a modification of the set-up, in order to utilize the subsequent sedimentation after flotation, such as more drainage time, wash water, and etc., enhanced separation results could be expected in the future projects.

Figure 22 presents the separation of Fe_2O_3-SiO_2 mixture by HTAB CGA flotation system (Experiment G-2).

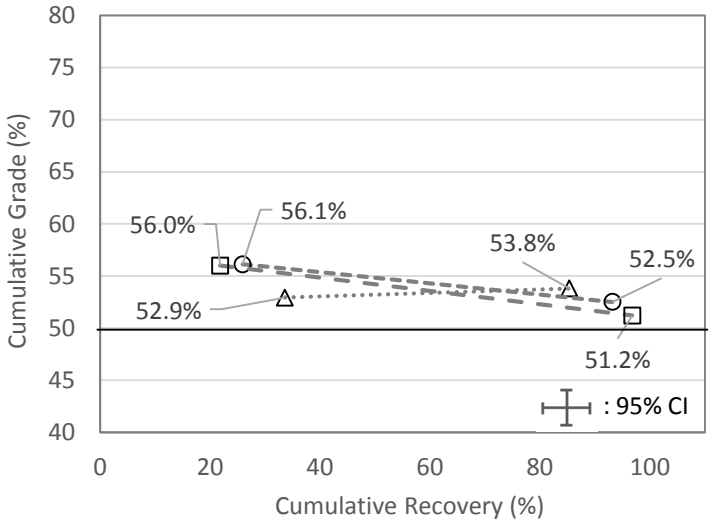

Figure 22. Grade-recovery of Fe_2O_3 by HTAB CGA flotation: ···△···, pH 3; -○-, pH 7; - □ -, pH 10 (data label presents grade, and solid line presents feed grade)

The slope of pH 3 data is positive and distinguished from the negative slopes of pH 7 and 10, and the positive slope implicates that Fe_2O_3 was detached from HTAB CGA while drainage of froth. As observed at pH 3 of Experiment C-3, it seems likely that Fe_2O_3 particles of highly positive surface charge were repelled by the cationic HTAB CGA.

The results form Figure 19, 20, and 22 are compared in Table 12, with the zeta potential measurements (Experiments E-1 and E-2), single mineral recoveries (Experiments C-3 and C-4), and bi-mineral separation (Experiment G-2).

Table 12: Comparison of synthetic mineral flotation results by HTAB CGA

pH	Measurements	Experiments E-1, and C-3 (Fe_2O_3)	Experiments E-2, and C-4 (SiO_2)	Experiment G-2 (bi-mineral cumulative results)
pH 3	Natural zeta potential	+ 55.4 mV	- 38.4 mV	Grade: 53.8 % Recovery: 85.3 %
	Recovery	2.5 %	89.4 %	
pH 7	Natural zeta potential	+ 18.6 mV	- 66.1 mV	Grade: 52.5 % Recovery: 93.2 %
	Recovery	69.6 %	93.3 %	
pH 10	Natural zeta potential	- 24.1 mV	- 75.1 mV	Grade: 51.2 % Recovery: 96.8 %
	Recovery	84.3 %	95.6 %	

From the summary results of single mineral recovery in Table 12, SiO_2 recovery was steadily high, but Fe_2O_3 recovery was varying depending on pH. The low recovery of Fe_2O_3 at pH 3 (Experiment C-3) was due to the repulsion between

positively charged Fe_2O_3 particles (+ 55.4 mV) and cationic HTAB CGA. This phenomena resulted in positive slope of grade-recovery charts at pH 3 (Figure 22) implicating that non-selectively entrained Fe_2O_3 particles were detached while froth were draining.

Figure 23 makes comparison between the cumulative recoveries of separation experiment with synthetic mineral mixtures (Experiment G-2) and the average of the respective recoveries with Fe_2O_3 and SiO_2 by HTAB CGA (Experiments C-3 and C-4). Both results showed comparable trend of increasing recovery as pH increases from pH 3 to pH 10. The similar observation was also found with natural minerals (Figure 30) that the recovery from separation experiments showed comparable trend with recoveries of respective minerals.

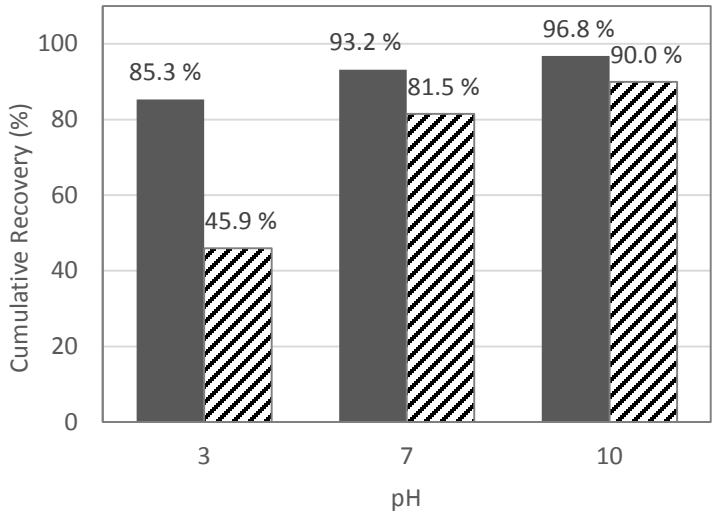

Figure 23. Comparison of cumulative recovery of binary mineral feeds (synthetic) separated by HTAB CGA and the average of respective recoveries of Fe_2O_3 and SiO_2: ■, bi-mineral separation (from Figure 22); ▨, average of Fe_2O_3 (Figure 19) and SiO_2 recovery (Figure 20)

4.4 Natural Minerals

4.4.1 Zeta potential of Hematite and Quartz

The zeta potentials of 3% w/w hematite (Experiment F-1) and 3% w/w quartz (Experiment F-2) suspensions were measured between pH 3 and 10, and the results are presented in Figure 24.

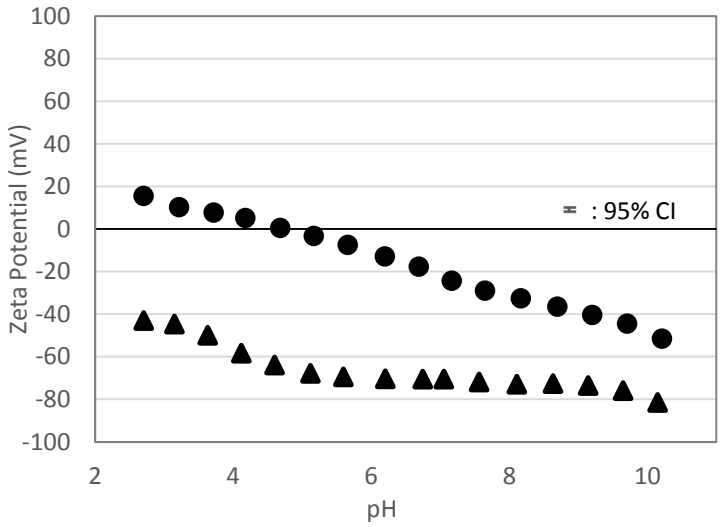

Figure 24. Zeta potential of hematite and quartz as a function of pH: ●, hematite; ▲, quartz

The natural pH and zeta potential were pH 7.1 and -24 mV for hematite and pH 6.0 and -70 mV for quartz. The zeta potential of hematite indicates an IEP of approximately pH 5.0. This corresponds to values quoted by Parks (1965) and Fuerstenau and Raghavan (2007). Across the pH range investigated, the zeta

potential of quartz remained negative. Extrapolation of the curve indicates that IEP would occur between the pH 2 and 3, if the trend is indeed followed. This postulated IEP value of quartz is consistent with the data referred by Parks (1965) and Fuerstenau and Raghavan (2007).

4.4.2 Anionic Surfactant (SDS) System

In Figure 25, the results of hematite flotation recovery by SDS CGA (Experiment D-1) are presented, and zeta potential measurements of hematite suspension at different SDS concentrations (Experiment F-1 and F-3) are compared. When hematite suspensions at pH 3 and pH 5 are floated by negatively charged CGA, the recoveries ranged from 50.5% recovery at pH 5 to 79.4 % recovery at pH 3.When the pH was increased to 10, the recoveries decreased to 25.7% at pH 7 and 10.0% at pH 10, thus pH dependency of hematite recovery was observed. When the variation of zeta potential with the addition of SDS surfactant to hematite suspension is considered, at pH 3 hematite and SDS interaction showed a good sign of SDS adsorption. Under these conditions, anionic SDS molecules adsorbed on the positively charged places of hematite surface, and this observation support the analysis from Section 4.3 that the attractive forces are generated between negatively charged SDS microbubbles and Fe_2O_3 particles. Therefore, in Experiment D-1, the attractive forces at pH 3 lead to high level of hematite recovery. On the other hand,

where a little evidence of adsorption is observed at pH 10, negatively charged hematite particles and anionic microbubbles appear to repel each other.

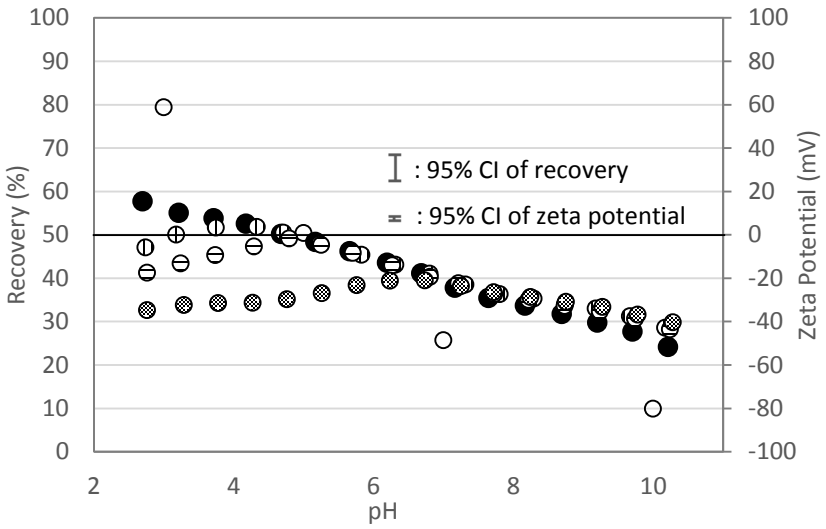

Figure 25. Hematite recoveries by SDS CGA flotation as a function of pH, and comparison of hematite zeta potential at different SDS concentrations: ○, hematite recovery; ●, hematite zeta potential; ◐, hematite zeta potential with 9.0 mg m^{-2} SDS; ⊖, hematite zeta potential with 14.5 mg m^{-2} SDS; ◍, hematite zeta potential with 31.1 mg m^{-2} SDS

The results of quartz flotation recovery by SDS CGA (Experiment D-2) and quartz zeta potential at different SDS concentrations (Experiments F-2 and F-4) are presented in Figure 26. The quartz recovery by SDS CGA was low with a maximum of 8.6% recovery (Experiment D-2), and there was little evidence of SDS adsorption, if any, on the surface of quartz particles (Experiments F-2 and F-4). The low recovery of quartz can be interpreted as a result of repulsive forces between

particles and microbubbles of like charges, which is in agreement with the observation with synthetic minerals from Experiment C-2 (Figure 16) and Experiment E-2 and E-4 (Figure 18) from Section 4.3.

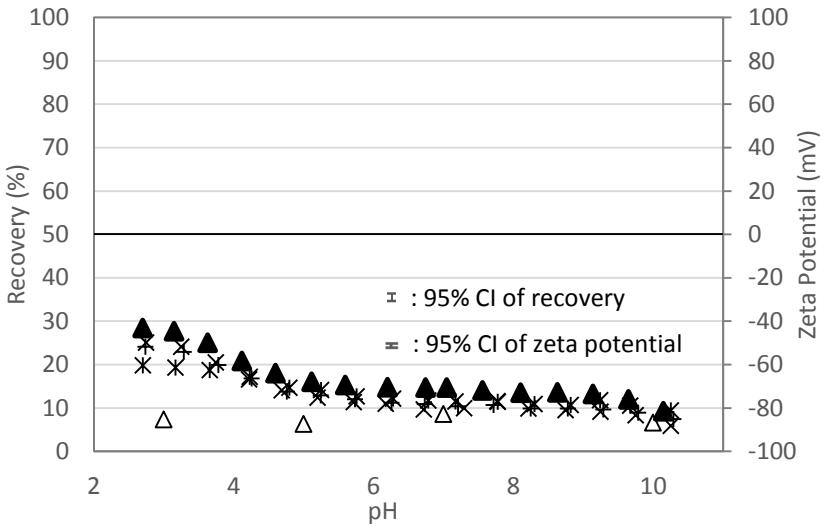

Figure 26. Quartz recoveries by SDS CGA flotation as a function of pH, and comparison of quartz zeta potential at different SDS concentrations: △, quartz recovery; ▲, quartz zeta potential; ×, quartz zeta potential with 11.8 mg m^{-2} SDS; +, quartz zeta potential with 19.0 mg m^{-2} SDS; ✳, quartz zeta potential with 40.7 mg m^{-2} SDS

SDS adsorption on hematite (Experiment F-3) showed pH dependency, which is driven by electrostatic properties of particles and surfactants, and a similar trend was observed in hematite recovery (Experiment D-1) when SDS CGA were used for flotation (Figure 25). When SDS surfactant was added into quartz suspension (Experiment F-4), the surfactant interaction showed little adsorption, if any, at all

the pH ranges studied. Furthermore, this phenomena could be correlated well with the low recovery of quartz by SDS CGA (Experiment D-2) as presented in Figure 26. When both results of particle-SDS adsorption (Experiments F-1 - F-4) and particle recovery by SDS CGA (Experiments D-1 and D-2) were compared, it is proposed that particle-SDS CGA interaction is driven by electrostatic properties of their surfaces.

4.4.3 Cationic Surfactant (HTAB) System

In Figure 27, the results of hematite flotation recovery by HTAB CGA (Experiment D-3) are presented and the zeta potential measurements of hematite with different HTAB concentrations (Experiments F-1 and F-5) are compared. The recovery of hematite is generally high with minimum of 91.3% recovery across the entire pH range.

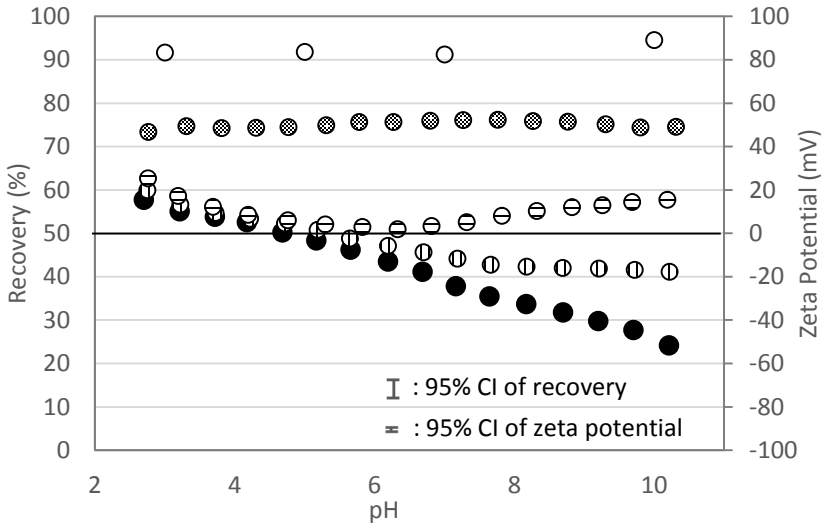

Figure 27. Hematite recoveries by HTAB CGA flotation as a function of pH, and comparison of hematite zeta potential at different HTAB concentrations: ○, hematite recovery; ●, hematite zeta potential; ◍, hematite zeta potential with 0.5 mg m^{-2} HTAB; ⊖, hematite zeta potential with 1.7 mg m^{-2} HTAB; ◍, hematite zeta potential with 6.1 mg m^{-2} HTAB

The variation of zeta potential measurements which is presented on the right hand y-axis of Figure 27 gives an indication of the HTAB adsorption on the surface of hematite across the pH range studied. Above the IEP, the attractive electrostatic interactions between negatively charged hematite and positively charged HTAB heads dominated the adsorption phenomena. Below the IEP, cationic HTAB molecules, however, adsorbed further on the surface of hematite particles even though the hematite has a positive zeta potential. The zeta potential of hematite suspension is below 20 mV, and the relatively low level of zeta potential means that there are enough negatively charged sites on the surface of hematite particles, on which HTAB molecules can adsorb. The more HTAB provided to the system, the greater the number of surfactant molecules that adsorb on the particles as a form of hemimicelles. As noted in Section 2.5.1, the generation of HTAB hemimicelles at higher concentration of surfactant provides sufficient sites for flotation to occur.

The results of quartz flotation recovery by HTAB CGA (Experiment D-4) and quartz zeta potential at different HTAB concentrations (Experiments F-2 and F-6) are shown in Figure 28. The quartz recovery by HTAB CGA was high, and HTAB showed good adsorption onto quartz, leading to a charge reversal across the entire pH range. The opposite charges of the quartz surface and HTAB head would form attractive forces and dominate the adsorption mechanism. These results are in a good agreement with the results with synthetic minerals as discussed in Section

4.3.3 (Experiments C-4, E-2, and E-6, the results of which are presented in Figure 20).

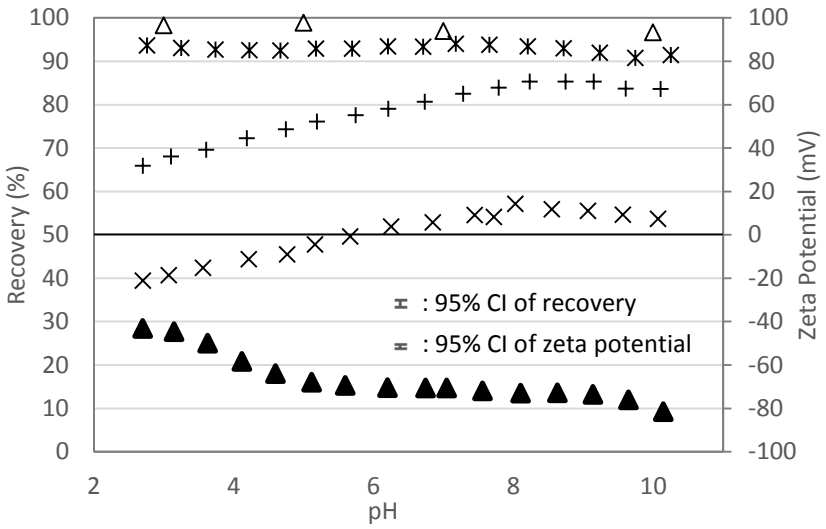

Figure 28. Quartz recoveries by HTAB CGA flotation as a function of pH, and comparison of quartz zeta potential at different HTAB concentrations: △, quartz recovery; ▲, quartz zeta potential; ×, quartz zeta potential with 0.7 mg m^{-2} HTAB; +, quartz zeta potential with 2.3 mg m^{-2} HTAB; ✳, quartz zeta potential with 7.9 mg m^{-2} HTAB

Good adsorption of HTAB on hematite occurred across the entire pH range studied (Experiments F-1 and F-5), and this observation correlated well with high recoveries of hematite when HTAB CGAs were used for the flotation (Experiment D-3) as shown in Figure 27. When HTAB was introduced to the quartz suspension, the surfactant showed high adsorption across the entire pH range (Experiments F-2

and F-6), and this could explain the mechanism of high recovery of quartz by HTAB CGA (Experiment D-4) as presented in Figure 28.

A strong positive correlation between particle-surfactant interaction (Experiments F-1 - F-6) and particle recovery by SDS CGA (Experiments D-1 and D-2) and by HTAB CGA (Experiments D-3 and D-4), leads to the proposed mechanism of how particles and CGA interact. The high degree of particle recovery was related to adsorption of surfactant to particles which is in agreement with electrostatic properties of particles and CGA. Further, lower levels of particle recovery can be associated to poor adsorption of surfactants to particle surface, which is also explained by their electrostatic interactions. This analysis is also consistent with the observations with synthetic minerals, such as surfactant adsorption (Experiments E-1 - E-6) and particle recovery by SDS CGA (Experiments C-1 and C-2) and by HTAB CGA (Experiments C-3 and C-4). Therefore it is believed that a particle is attached to a charged microbubble when they are driven attractively by electrostatic properties of each other, and that a particle is prevented from being attached to CGA when there exists repulsive electrostatic barrier due to their similar charge.

4.4.4 Separation of Natural Binary Fine Minerals

Figure 29 presents the separation of hematite-quartz mixture by SDS CGA flotation system (Experiment H-1). The feed was 50:50 mixture of the hematite concentrate (95.1% of iron (III) oxide contents) and quartz, therefore the iron (III) oxide content is 47.6% of the feed.

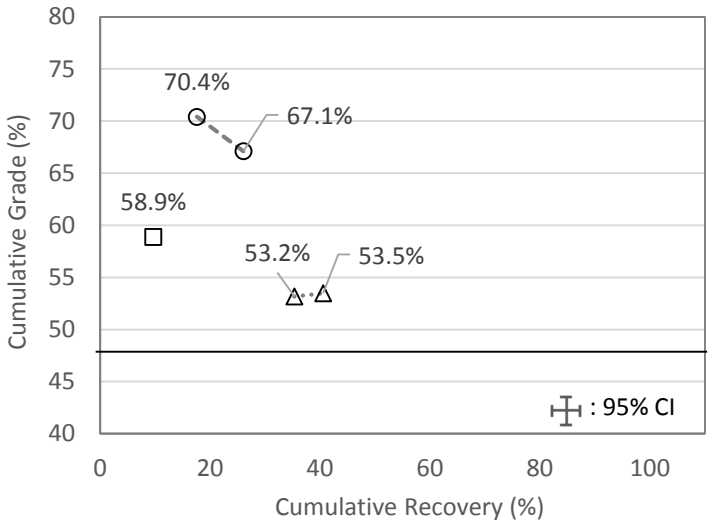

Figure 29. Grade-recovery of hematite by SDS CGA flotation: ···△···, pH 3; -·-○-·-, pH 7; - ⊟ -, pH 10 (data label presents grade, and solid line presents feed grade)

Among the four sets of separation experiments (Experiments G-1, G-2, H-1, and H-2), Experiment H-1 reported relatively low cumulative recovery (9.7% - 40.6%) and higher cumulative grade (53.5% - 67.1%). On the other hand, the Experiments G-1, G-2, and H-2 (presented in Figure 21, 22, and 31, respectively) showed high

cumulative recovery arriving at nearly all the feed amount and low cumulative grade converging to the feed grade.

The observations that were not be quantified in this analysis were stability and drainage of CGA froth, which could be linked to the rise velocity of CGA froth. Although CGA dispersions were pumped into the flotation column at the same volumetric rate per unit time, the rise velocity of froth from Experiment H-1 was slower than those of Experiments G-1, G-2, and H-2. Accordingly, more fragile froth was foamed and better drainage were observed from Experiment H-1, which reported relatively lower recovery and higher grade. In case of pH 10 from Figure 29, the froth could not rise to the lip of the column, not generating any overflows, hence the only marker in Figure 29 for pH 10 represents the data of the froth. Due to the limited experimental design for this project, the effect of stability and drainage of CGA froth has not been examined with regards to its consequences for recovery and grade. Therefore the effect of these factors to the separation process by CGA flotation should be further investigated at the future studies.

The results of Figure 25, 26, and 29 were compared in Table 13, with the zeta potential measurements (Experiments F-1 and F-2), single mineral recoveries (Experiments D-1 and D-2), and bi-mineral separation (Experiment H-1).

Table 13: Comparison of natural mineral flotation results by SDS CGA

pH	Measurements	Experiments F-1 and D-1 (hematite)	Experiments F-2 and D-2 (quartz)	Experiment H-1 (bi-mineral cumulative results)
pH 3	Natural zeta potential	+ 12.8 mV	- 43.9 mV	Grade: 53.5 % Recovery: 40.6 %
	Recovery	79.4 %	7.4 %	
pH 7	Natural zeta potential	- 21.1 mV	- 70.6 mV	Grade: 67.1 % Recovery: 26.1 %
	Recovery	25.7 %	8.6 %	
pH 10	Natural zeta potential	- 48.1 mV	- 81.5 mV	Grade: 58.9 % Recovery: 9.7 %
	Recovery	10.0 %	6.7 %	

Although the level of aggregation and flocculation was not examined with the scope of this work, making an assumption on the anticipated interactions between hematite and quartz based on the zeta potential analysis would be helpful to interpret the results of Experiment H-1. Analyzing to the results of pH 3 in Table 13, the opposite signs of zeta potentials imply that flocculation of hematite and quartz would be anticipated. Further, low positive values (+ 12.8 mV) of hematite zeta potential and a moderate level of negative value of quartz (- 43.9 mV) could enhance the aggregation and flocculation of hematite and quartz particles. Therefore 53.5% of iron (III) oxide grade at pH 3 may be due to large amounts of quartz recovered unselectively when hematite particles were floated by SDS CGA.

The high grade (67.1%) at pH 7 from Experiment H-1 could be related to the lower levels of flocculation of hematite and quartz due to the same sign of particles and dispersed quartz particles due to high negativity of quartz zeta potential (- 70.6 mV). Although hematite was negatively charged, there could be enough number of positively charged spots for the anionic SDS CGA to recover 26.1% of hematite particles. The grade at pH 10 is less meaningful as recovery is very low due to the repulsion between negatively charged particles and anionic SDS CGA. Although the assumptions of aggregation and flocculation should be further substantiated with future experiments, the current analysis provided reasonable interpretation of Experiment H-1 that selective attachment was achieved by utilizing electrostatic interactions of particles and CGA.

Figure 30 summaries the cumulative recoveries of separation experiment with natural mineral mixtures (Experiment H-1) and the average of the respective recoveries of hematite and quartz by SDS CGAs (Experiments D-1 and D-2). Both results showed comparable trend of decreasing recovery as pH increases from pH 3 to pH 10. The similar observation was also found with synthetic minerals (Figure 23) that the recovery from separation experiments showed comparable trend with recoveries of respective minerals. Both observations with synthetic and natural minerals further supports that mechanism of binary feed separation being attributed to the respective mechanism of single feed recovery by CGAs.

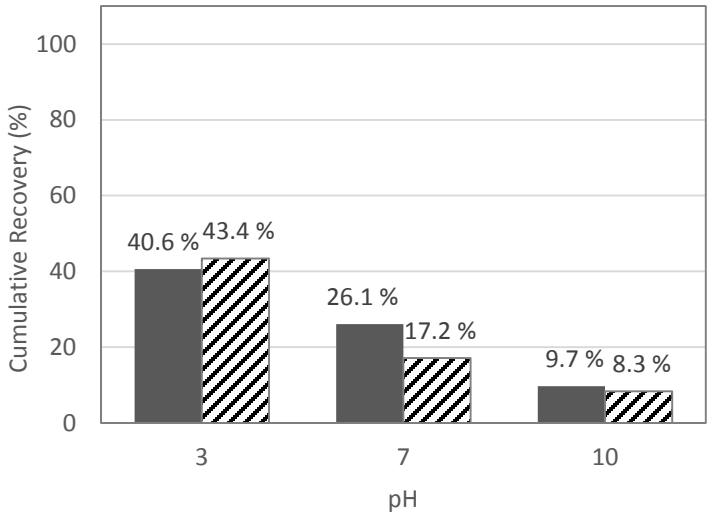

Figure 30. Comparison of cumulative recovery of binary mineral feeds (natural) separated by SDS CGA and the average of respective recoveries of hematite and quartz: ■, bi-mineral separation (from Figure 29); ▨, average of hematite (Figure 25) and quartz recovery (Figure 26)

Figure 31 presents separation results of binary natural minerals by HTAB CGA flotation (Experiment H-2). As seen from the high recoveries of single mineral experiments (minimum 91.3% and 96.7% recoveries from Experiments D-3 and D-4 respectively), HTAB CGA react attractively for both types of minerals, resulting in low separation. At pH 10, the flotation starts with high grades of overflow, probably with a help of dispersed status of hematite (- 48.1 mV zeta potential) and quartz (- 81.5 mV zeta potential), but it ends up with recovering everything because cationic HTAB CGA attracts negatively charged hematite and quartz indifferently.

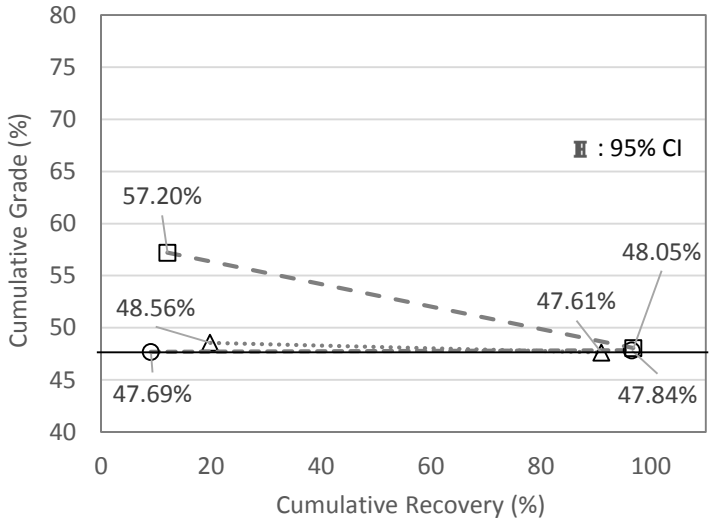

Figure 31. Grade-recovery of hematite by HTAB CGA flotation: ···△···, pH 3; -○-, pH 7; - □ -, pH 10 (data label presents grade, and solid line presents feed grade)

Although the relative behavior of two types of particles in the binary feeds were not directly studied, current studies of single mineral recovery and zeta potential measurements provided a consistent explanation on the results of separation experiments. Therefore it was concluded that CGA separation of natural minerals were mainly driven by electrostatic properties of hematite, quartz, and CGAs, and selective flotation was achieved.

5 Conclusions and Recommendations for Future Work

5.1 Conclusions

The CGA flotation system operated successfully for recovery experiments with single mineral feed, and both sets of synthetic particles and natural minerals showed strong correlations with recovery experiments (Experiments C-1 - C-4, and D-1 - D-4) and surfactant adsorption experiments (Experiments E-1 - E-6 and F-1 - F-6). High level of particle recovery was related to good adsorption of surfactant to the surface of particles, and this phenomena was in agreement with electrostatic attractions between particles and CGAs. When low levels of particle recovery were observed, it was associated to the poor adsorption of surfactant to the surface of particles, which is explained by the repulsive interactions of similar charge.

The results of separating binary mineral feeds (Experiments G-1, G-2, H-1, and H-2) were explained using the results of single mineral recovery experiments and zeta potential measurements. When the selective attachment of valuable (Fe_2O_3 or hematite) was expected based on the recovery experiments of single mineral feeds, negative slopes were observed from the grade-recovery charts of valuables, implicating that non-selectively entrained SiO_2 (or quartz) was detached while froth drained. Also the opposite case of positive slope was observed from Experiment G-2, implicating that entrained Fe_2O_3 was drained from the froth made of HTAB CGA.

The recovery from binary feeds was closely correlated to the average amount of recoveries of respective single mineral experiments (Figure 23, and 30), which further supports that mechanism of binary feeds separation being attributed to the respective mechanisms of single feed recovery results.

The highest grade was achieved when both types of composing particles were like-charged (67.1% grade at pH 7 in Experiment H-1), and it is proposed that a lower degree of flocculation of both materials enables more selective separation by CGA flotation.

The interaction between fine particles and CGAs is dependent on the electrostatic properties of particles and the charged microbubbles. Studies of single minerals provided a consistent rationale to explain the results of binary mineral separation experiments by CGA flotation. The CGA separation was driven by electrostatic interactions between feed composing materials and CGAs, and selective attachment was achieved.

5.2 Recommendations for Future Work

Aggregation and flocculation of the particles should be studied to better understand separation mechanism of CGA flotation. The highest grade was achieved when both types of composing particles had similar charge (67.1% grade at pH 7 in Experiment H-1), and it is proposed that a lower degree of flocculation of both materials enables more selective separation by CGA flotation. Currently measurements of particle aggregation and flocculation were not conducted within the scope of this project, therefore detailed measurements of particle aggregation and flocculation could further substantiate the rationale behind observed results.

Enhanced separation results are expected when CGA flotation system is optimized for the respective experiments. Subsequent sedimentation of entrained particles was observed from the overflow and froth after their collection (Experiment G-1), and the high grade of Experiment H-1 was related to more drainage of froth. These observations support the potential of enhanced separation, but the current CGA flotation set-ups could not utilize these phenomena. Adoption of wash water or more drainage time would enable the utilization of subsequent sedimentation of entrained particles. In addition, the adjustment of operating parameters such as CGA pumping speed or surfactant concentration will modify stability and drainage of CGA froth, which will contribute to optimal recovery-grade results. Currently, CGA flotation set-ups are for the maximum recovery of single mineral feeds and

the same set-up is used for the separation experiments to maintain consistency between each type of experiments. Therefore further optimization for the separation experiments has a potential for enhanced separation results.

References

Adamson, A.W., Gast, A.P., *Physical chemistry of surfaces.* 1967, Interscience Publishers, New York

Ananthapadmanabhan, K.P., Somasundaran, P., Acid-soap formation in aqueous oleate solutions. Journal of Colloid and Interface Science, 1988, **122(1)**, 104-109.

Aplan, F., Fuerstenau, D., Principles of nonmetallic mineral flotation. Froth Flotation, 1962, **50**, 170-214.

Ben-Naim, A., Wilf, J., Yaacobi, M., Hydrophobic interaction in light and heavy water. The Journal of Physical Chemistry, 1973, **77(1)**, 95-102.

Bhakta, A., Ruckenstein, E., Decay of standing foams: drainage, coalescence and collapse. Advances in Colloid and Interface Science, 1997, **70**, 1-124.

Bhatia, D., Goel, G., Bhimania, S.K., Bhaskarwar, A.N., Characterization and drainage kinetics of colloidal gas aphrons. AIChE Journal, 2005, **51(11)**, 3048-3058.

Bikerman, J.J., *Foams: theory and industrial applications*. 1953, Reinhold Publishing Corp., New York.

Bogdanov, O., Yeropkin, Y., Koltunova, T., Khobotova, N., Shtchukina, N., 1973. Hydroxamic acids as collectors in the flotation of wolframite, cassiterite and pyrochlore, In *Proceedings X International Mineral Processing Congress, IMM, London, UK*, p. 533.

Boonamnuayvitaya, V., Jutaporn, P., Sae-ung, S., Jarudilokkul, S., Removal of pyrene by colloidal gas aphrons of a biodegradable surfactant. Separation and Purification Technology, 2009, **68(3)**, 411-416.

Chadwick, J., Flotation: far from sinking. Mining Magazine, 2003, **188(3)**, 102-110.

Chang, C., Substituted starches in amine flotation of iron ore. Trans. AIME, 1954, **199**, 922-924.

Chernyshova, I.V., Rao, K.H., Vidyadhar, A., Shchukarev, A.V., Mechanism of adsorption of long-chain alkylamines on silicates. A Spectroscopic Study. 1. Quartz. Langmuir, 2000, **16(21)**, 8071-8084.

Chernyshova, I.V., Rao, K.H., Vidyadhar, A., Shchukarev, A.V., Mechanism of adsorption of long-chain alkylamines on silicates: A Spectroscopic Study. 2. Albite. Langmuir, 2001, **17(3)**, 775-785.

Choi, Y.J., Kim, Y.J., Nam, K., Enhancement of aerobic biodegradation in an oxygen-limiting environment using a saponin-based microbubble suspension. Environmental Pollution, 2009, **157(8–9)**, 2197-2202.

Ciriello, S., Barnett, S.M., Deluise, F.J., Removal of heavy metals from aqueous solutions using microgas dispersions. Separation Science and Technology, 1982, **17(4)**, 521-534.

Cooper, M., Scott, D., Dahlke, R., Finch, J., Gomez, C., Impact of air distribution profile on banks in a Zn cleaning circuit. CIM Bulletin, 2004, **97(1083)**, 1-6.

Cornell, R.M., Schwertmann, U., *The Iron Oxides: Structure, Properties, Reactions, Occurrences and Uses*. 1996, Wiley-VCH, New York.

Couto, H.J.B., Massarani, G., Biscaia Jr, E.C., Sant'Anna Jr, G.L., Remediation of sandy soils using surfactant solutions and foams. Journal of Hazardous Materials, 2009, **164(2–3)**, 1325-1334.

Dashevsky, V.G., Sarkisov, G.N., The solvation and hydrophobic interaction of non-polar molecules in water in the approximation of interatomic potentials: The Monte Carlo method. Molecular Physics, 1974, **27(5)**, 1271-1290.

Dobby, G., Finch, J., Particle size dependence in flotation derived from a fundamental model of the capture process. International Journal of Mineral Processing, 1987, **21(3–4)**, 241-260.

Dobby, G., Finch, J., Column flotation: A selected review, part II. Minerals Engineering, 1991, **4(7–11)**, 911-923.

Dobson, K.D., Roddick-Lanzilotta, A.D., McQuillan, A.J., An in situ infrared spectroscopic investigation of adsorption of sodium dodecylsulfate and of cetyltrimethylammonium bromide surfactants to TiO_2, ZrO_2, Al_2O_3, and Ta_2O_5 particle films from aqueous solutions. Vibrational Spectroscopy, 2000, **24(2)**, 287-295.

Egan, J.R., Fairweather, M.J., Meekel, W.A., Application of Column Flotatinn to Lead and Zinc Beneficiation at Cominco,. Column Flotation'88 (Ed., Sastry, K.V.S.), SME annual meeting, 1988, 19-26.

Fan, A., Somasundaran, P., Turro, N.J., Adsorption of alkyltrimethylammonium bromides on negatively charged alumina. Langmuir, 1997, **13(3)**, 506-510.

Feng, W., Singhal, N., Swift, S., Drainage mechanism of microbubble dispersion and factors influencing its stability. Journal of Colloid and Interface Science, 2009, **337(2)**, 548-554.

Finch, J., Dobby, G., Column flotation: A selected review. Part I. International Journal of Mineral Processing, 1991, **33(1–4)**, 343-354.

Fuda, E., Jauregi, P., An insight into the mechanism of protein separation by colloidal gas aphrons (CGA) generated from ionic surfactants. Journal of chromatography. B, Analytical technologies in the biomedical and life sciences, 2006, **843(2)**, 317-326.

Fuerstenau, D., Interfacial processes in mineral/water systems. Pure and Applied Chemistry, 1970, **24(1)**, 135-164.

Fuerstenau, D., Fine particle flotation. Fine particles processing, 1980, **1**, 669-705.

Fuerstenau, D., Healy, T.W., Somasundaran, P., The role of the hydrocarbon chain of alkyl collectors in flotation. Trans. AIME, 1964, **229**, 321-325.

Fuerstenau, D., Raghavan, S., The surface and crystal chemistry of silicate minerals and their flotation behavior. Freiberger Forschungsh. A, 1978, **593**, 75-109.

Fuerstenau, D., Gaudin, A., Miaw, H., Iron oxide slime coatings in flotation. Transactions of the American Institute of Mining and Metallurgical Engineers, 1958, **211(JAN)**, 792-795.

Fuerstenau, D., Raghavan, S., Some aspects of flotation thermodynamics. Froth Flotation, A Century of Innovation, ed. Fuerstenau, M., Jameson, G., and Yoon, R.-H., Society of Mining, Metallurgy and Exploration (SME), Colorado, USA, 2007, 95-132.

Fuerstenau, M., Oxide and silicate flotation. Flotation Science and Engineering, 1995, 89-126.

Fuerstenau, M., Harper, R., Miller, J., Hydroxamate vs. fatty acid flotation of iron oxide. Trans. Soc. Mining Eng. AIME, 1970, **247(1)**, 69-73.

Fuerstenau, M., Rice, D., Flotation characteristics of pyrolusite. AIME Trans, 1968, **241**, 453-457.

Fuerstenau, M., Insoluble oxides and silicates. Froth Flotation, A Century of Innovation, ed. Fuerstenau, M., Jameson, G., and Yoon, R.H., Society of Mining, Metallurgy and Exploration (SME), Colorado, USA, 2007, 466-474.

Fuerstenau, M., Palmer, B., Anionic flotation of oxides and silicates. Flotation--A. M. Gaudin Memorial, 1976.

Gaudin, A., Groh, J.O., Henderson, H., Effect of particle size on flotation. Technical Publication, 1931**(414)**.

Grahame, D.C., The Electrical Double Layer and the Theory of Electrocapillarity. Chemical Reviews, 1947, **41(3)**, 441-501.

Greene, E.W., Duke, J.B., Selective froth flotation of ultrafine minerals or slimes. Trans. AIME, 1962, **223**, 389-395.

Hadler, K., Cilliers, J., The relationship between the peak in air recovery and flotation bank performance. Minerals Engineering, 2009, **22(5)**, 451-455.

Hankins, N.P., O'Have, J.H., Harwell, J.H., Modeling effects of pH and counterions on surfactant adsorption at the oxide/water interface. Industrial & Engineering Chemistry Research, 1996, **35(9)**, 2844-2855.

Israelachvili, J., Pashley, R., The hydrophobic interaction is long range, decaying exponentially with distance. Nature, 1982, **300(5890)**, 341-342.

Iwasaki, I., 1983. Iron Ore Flotation, Theory and Practice, Gaudin Lecture, In *1982 Annual AIME Meeting, AIME Transactions*, pp. 622-631.

Iwasaki, I., Cooke, S., Choi, H., Flotation characteristics of hematite, goethite, and activated quartz with 18-carbon aliphatic acids and related compounds. American Institute of Mining, Metallurgical and Petroleum Engineers. Transactions, 1960a, **217**, 237-244.

Iwasaki, I., Cooke, S., Choi, H., Flotation of cummingtonite. Trans. AIME, 1961, **220**, 394.

Iwasaki, I., Cooke, S., Colombo, A.F., Flotation characteristics of goethite. 1960b.

Jarudilokkul, S., Rungphetcharat, K., Boonamnuayvitaya, V., Protein separation by colloidal gas aphrons using nonionic surfactant. Separation and Purification Technology, 2004, **35(1)**, 23-29.

Jauregi, P., Dermiki, M., *Separation of value-added bioproducts by colloidal gas aphrons (CGA) flotation and applications in the recovery of value-added food products.* 2010, Woodhead Publishing Limited, Cambridge.

Jauregi, P., Gilmour, S., Varley, J., Characterisation of colloidal gas aphrons for subsequent use for protein recovery. The Chemical Engineering Journal and the Biochemical Engineering Journal, 1997, **65(1)**, 1-11.

Jauregi, P., Mitchell, G.R., Varley, J., Colloidal gas aphrons (CGA): Dispersion and structural features. AIChE Journal, 2000, **46(1)**, 24-36.

Johnson, D., Hilal, N., Waters, K., Hadler, K., Cilliers, J., Measurements of Interactions between Particles and Charged Microbubbles Using a Combined Micro- and Macroscopic Strategy. Langmuir, 2009, **25(9)**, 4880-4885.

Johnson, N.W., Liberated 0–10μm particles from sulphide ores, their production and separation—Recent developments and future needs. Minerals Engineering, 2006, **19(6–8)**, 666-674.

Johnson, R.E., Conflicts between Gibbsian thermodynamics and recent treatments of interfacial energies in solid-liquid-vapor. The Journal of Physical Chemistry, 1959, **63(10)**, 1655-1658.

Kahlweit, M., Ostwald ripening of precipitates. Advances in Colloid and Interface Science, 1975, **5(1)**, 1-35.

Kauzmann, W., 1959. Some Factors in the Interpretation of Protein Denaturation, In *Advances in Protein Chemistry*, eds. Anfinsen, C.B., Anson, M.L., Bailey, K., Edsall, J.T.. Academic Press, pp. 1-63.

Ketkar, D.R., Mallikarjunan, R., Venkatachalam, S., Electroflotation of quartz fines. International Journal of Mineral Processing, 1991, **31(1–2)**, 127-138.

Koehler, S.A., Hilgenfeldt, S., Stone, H.A., A generalized view of foam drainage: Experiment and Theory. Langmuir, 2000, **16(15)**, 6327-6341.

Laskowski, J., Kitchener, J.A., The hydrophilic—hydrophobic transition on silica. Journal of Colloid and Interface Science, 1969, **29(4)**, 670-679.

Leja, J., Poling, G., 1960. On the interpretation of contact angle, In *Proceedings of the 5th Mineral Processing Congress*, p. 325.

Matis, K.A., Gallios, G.P., 1986. Dissolved-Air and Electrolytic Flotation, In *Mineral Processing at a Crossroads*, eds. Wills, B.A., Barley, R.W. Springer Netherlands, pp. 37-69.

Montes-Sotomayor, S., Houot, R., Kongolo, M., Flotation of silicated gangue iron ores: Mechanism and effect of starch. Minerals Engineering, 1998, **11(1)**, 71-76.

Moshkelani, M., Amiri, M.C., Electrical conductivity as a novel technique for characterization of colloidal gas aphrons (CGA). Colloids and Surfaces A: Physicochemical and Engineering Aspects, 2008, **317(1–3)**, 262-269.

Musić, S., Wolf, R.H.H., Sorption of microamounts of gallium (III) on $Fe(OH)_3$ and Fe_2O_3 precipitates. Mikrochim Acta, 1979, **71(1-2)**, 87-94.

Noble, M., Brown, A., Jauregi, P., Kaul, A., Varley, J., Protein recovery using gas–liquid dispersions. Journal of Chromatography B: Biomedical Sciences and Applications, 1998, **711(1–2)**, 31-43.

Palmer, B., Fuerstenau, M., Aplan, F., Mechanisms involved in the flotation of oxides and silicates with anionic collectors. Transactions AIME, 1975, **258**, 261-263.

Park, J.Y., Choi, Y.J., Moon, S., Shin, D.Y., Nam, K., Microbubble suspension as a carrier of oxygen and acclimated bacteria for phenanthrene biodegradation. Journal of Hazardous Materials, 2009, **163(2–3)**, 761-767.

Parks, G.A., The isoelectric points of solid oxides, solid hydroxides, and aqueous hydroxo complex systems. Chemical Reviews, 1965, **65(2)**, 177-198.

Parks, G.A., Bruyn, P.D., The zero point of charge of oxides. The Journal of Physical Chemistry, 1962, **66(6)**, 967-973.

Rao, K.H., Forssberg, K.S.E., Chemistry of iron oxide flotation. Froth Flotation, A Century of Innovation, ed. Fuerstenau, M., Jameson, G., and Yoon, R.H., Society of Mining, Metallurgy and Exploration (SME), Colorado, USA, 2007, 498-513.

Rao, S.R., *Surface chemistry of froth flotation*. 2004, Kluwer Academic/Plenum Publishers, New York.

Reay, D., Ratcliff, G.A., Removal of fine particles from water by dispersed air flotation: Effects of bubble size and particle size on collection efficiency. The Canadian Journal of Chemical Engineering, 1973, **51(2)**, 178-185.

Roy, D., Valsaraj, K.T., Kottai, S.A., Separation of organic dyes from wastewater by using colloidal gas aphrons. Separation Science and Technology, 1992, **27(5)**, 573-588.

Save, S.V., Pangarkar, V.G., Characterisation of colloidal gas aphrons. Chemical Engineering Communications, 1994, **127(1)**, 35-54.

Sebba, F.F., *Foams and biliquid foams - aphrons*. 1987, John Wiley & Sons Ltd.

Shergold, H.L., Mellgren, O., Concentration of minerals at the oil-water interface: hematite-isoctane-water system in the presence of sodium dodecyl sulphate. Trans. IMM, 1969, **78**, C121-C132.

Sjoberg, S., Ohman, L.O., Equilibrium and structural studies of silicon (IV) and aluminium (III) in aqueous solution. Part 13. A potentiometric and 27Al nuclear magnetic resonance study of speciation and equilibria in the aluminium (III)-oxalic acid-hydroxide system. Journal of the Chemical Society, Dalton Transactions, 1985**(12)**, 2665-2669.

Smith, R.W., L Scott, J., Mechanisms of dodecylamine flotation of quartz. Mineral Processing and Extractive Metallurgy Review, 1990, **7(2)**, 81-94.

Somasundaran, P., An overview of the ultrafine problem, In *Mineral Processing at a Crossroads*. Springer, 1986, 1-36.

Sposito, Garrison. *The surface chemistry of natural particles.* Vol. 389. New York: Oxford University Press, 2004.

Sresty, G.C., Somasundaran, P., Selective flocculation of synthetic mineral mixtures using modified polymers. International Journal of Mineral Processing, 1980, **6(4)**, 303-320.

Sutherland, K.L., Physical Chemistry of Flotation. XI. Kinetics of the Flotation Process. The Journal of Physical and Colloid Chemistry, 1948, **52(2)**, 394-425.

Tao, Y., Liu, J., Yu, S., Tao, D., Picobubble Enhanced Fine Coal Flotation. Separation Science and Technology, 2006, **41(16)**, 3597-3607.

Torrecilla, P.J., Colloidal gas aphrons (CGA) : a novel approach to protein recovery. University of Reading, 1997.

Trahar, W.J., A rational interpretation of the role of particle size in flotation. International Journal of Mineral Processing, 1981, **8(4)**, 289-327.

Trahar, W.J., Warren, L.J., The flotability of very fine particles - A review. International Journal of Mineral Processing, 1976, **3(2)**, 103-131.

Wakamatsu, T., Fuerstenau, D., Effect of alkyl sulfonates on the wettability of alumina. Transactions of the American Institute of Mining, Metallurgical and Petroleum Engineers (Society of Mining Engineers), 1973, **254**.

Wang, Y.H.C., Somasundaran, P., A study of carrier flotation of clay. Fine Particles Processing, 1980, **2**, 1112-1128.

Waters, K., Hadler, K., Cilliers, J., The flotation of fine particles using charged microbubbles. Minerals Engineering, 2008, **21(12-14)**, 918-923.

Wills, B.A., *Wills' mineral processing technology an introduction to the practical aspects of ore treatment and mineral recovery*. 2006, Elsevier/BH, Amsterdam; Boston; London.

Xu, Q., Nakajima, M., Ichikawa, S., Nakamura, N., Shiina, T., A comparative study of microbubble generation by mechanical agitation and sonication. Innovative Food Science & Emerging Technologies, 2008, **9(4)**, 489-494.

Yalcin, T., Byers, A., Dissolved Gas Flotation in Mineral Processing. Mineral Processing and Extractive Metallurgy Review, 2006, **27(2)**, 87-97.

Yan, Y.L., Qu, C.T., Zhang, N.S., Yang, Z.G., Liu, L., A study on the kinetics of liquid drainage from colloidal gas aphrons (CGAs). Colloids and Surfaces A: Physicochemical and Engineering Aspects, 2005, **259(1–3)**, 167-172.

Yoon, R.H., Microbubble flotation. Minerals Engineering, 1993, **6(6)**, 619-630.

Yoon, R.H., The role of hydrodynamic and surface forces in bubble–particle interaction. International Journal of Mineral Processing, 2000, **58(1–4)**, 129-143.

Yoon, R.H., Luttrell, G.H., The Effect of Bubble Size on Fine Particle Flotation. Mineral Processing and Extractive Metallurgy Review, 1989, **5(1-4)**, 101-122.

Yopps, J.A., Fuerstenau, D.W., The zero point of charge of alpha-alumina. Journal of Colloid Science, 1964, **19(1)**, 61-71.

Appendix

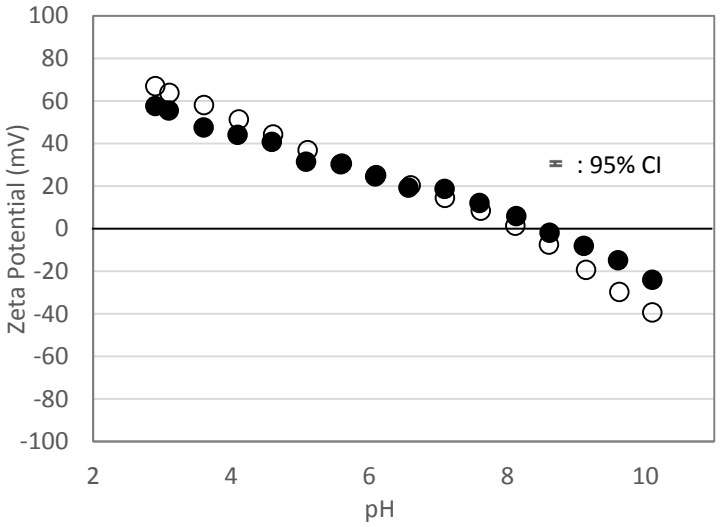

Figure A-1. Zeta potential of Fe_2O_3 at different concentrations: ●, 3% Fe_2O_3; ○, 10% Fe_2O_3

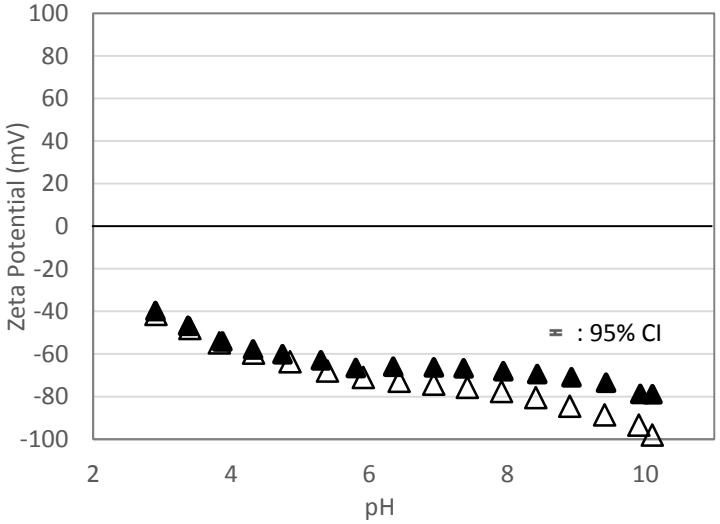

Figure A-2. Zeta potential of SiO_2 at different concentrations: ▲, 3% SiO_2; △, 10% SiO_2

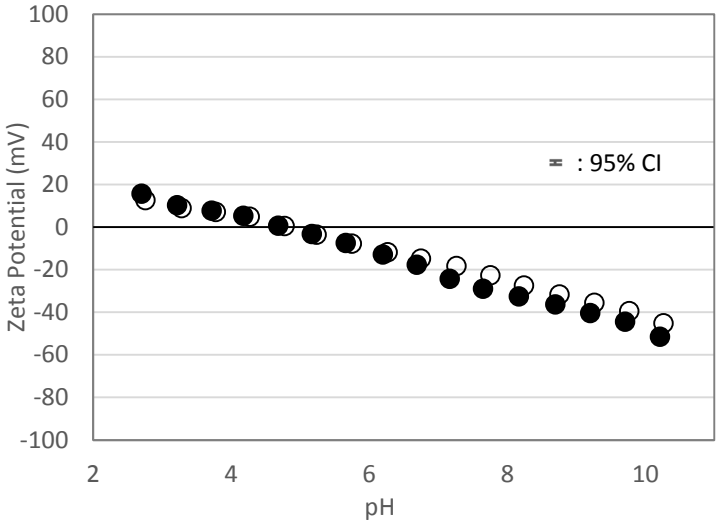

Figure A-3. Zeta potential of hematite at different concentrations: ●, 3% hematite; ○, 10% hematite

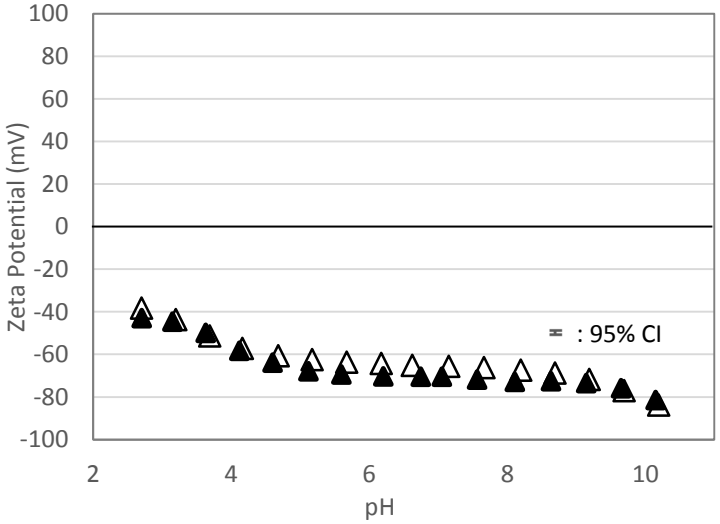

Figure A-4. Zeta potential of quartz at different concentrations: ▲, 3% quartz; △, 10% quartz